

Chapter 11 HELIUM-COOLED REFRACTORY ALLOYS FIRST WALL AND BLANKET

11.1 Introduction

Under the APEX program, the goal for the helium-cooled system design task is to evaluate and recommend robust high-power density refractory alloy, helium-cooled first wall and blanket design options, and to recommend and initiate tests to address critical issues. With the projected high allowable operating temperature of the refractory alloy, it has the potential of leading to a high thermal efficiency reactor design. We initiated our task by designing for an average neutron wall loading of 7 MW/m^2 , a surface heat flux of 2 MW/m^2 , and a peaking factor of 1.4. To meet these severe design parameters, we evaluated the use of refractory alloys like Ta, Mo, W, Nb, and V alloys in 1998 and performed the preliminary design of the W-alloy first wall and blanket concept in 1999. One critical issue for the design is the lack of irradiated design data for the W-alloy, which is projected to have a loss in ductility at low neutron fluence. To handle this lack of data, we estimated the properties of W-5Re alloy and evaluated the design by using different projected mechanical design criteria. We also evaluated the issue of material compatibility. For the first wall heat transfer design, we evaluated the possible use of porous medium and swirl tube options. Thermal hydraulics, nuclear, activation; and safety designs and analysis were also performed. We selected the use of high-pressure helium coolant at 12 MPa. The gross thermal efficiency of a closed cycle gas turbine (CCGT) power conversion system (PCS) was then determined. We then used these results and applied them to a system code design to estimate the cost of electricity (COE). Critical issues of this first wall and blanket design were also identified. Results of these evaluations are presented in this chapter.

11.2 Structural Material Selection and Compatibility Issues

A key element in the design of high performance, high power density helium-cooled first wall and blanket system is the selection of structural material. This section summarizes the evaluation and selection of refractory alloys and addresses the possibility of controlling the concentration of oxygen impurities in the helium stream to avoid the potential serious problem of material compatibility.

11.2.1 structural material selection — The proposed high operating temperatures ($\sim 1000^\circ\text{C}$) for the structure in the high power density helium-cooled concept severely limits the choice of structural materials. This eliminates the use of vanadium alloys, SiC/SiC composites, and all steels. We evaluated the use of refractory alloys like Ta, Mo, W, Nb and V alloys in 1998. Pure tungsten or tungsten alloyed with $\sim 5\%$ Re (to improve fabricability) appears to be a suitable candidate for the structure at these operating temperatures. The three main materials issues which help to determine the allowable operating temperature window for tungsten in a helium-cooled system are: (1) low temperature radiation embrittlement; (2) tensile strength, thermal creep, and helium embrittlement at high temperatures; and (3) high temperature corrosion associated with the formation of volatile oxides (due to oxygen impurities in the helium coolant). These issues are

summarized in the following and are discussed in more detail in the materials chapter (Chapter 13).

The unirradiated mechanical properties of tungsten are strongly dependent on thermomechanical processing conditions. The best tensile and fracture toughness properties are obtained in stress-relieved material. The strength of recrystallized tungsten is less than half that of stress-relieved tungsten at temperatures between 20° and 1300°C, and the ductile to brittle transition temperature (DBTT) of recrystallized W (>400°C for precracked fracture toughness specimens) is significantly higher than that of stress-relieved tungsten (~200°C). Since data are not available on the possibility of radiation-enhanced recrystallization of W, and also to account for the presence of welds in the structure, the current preliminary design is based on recrystallized mechanical properties in order to be conservative. The fracture toughness of unirradiated tungsten is relatively low compared to many other structural materials (*e.g.*, ~30 MPa-m^{1/2} at 1000°C).

There are no known mechanical properties data on tungsten or tungsten alloys at irradiation and test temperatures above ~800°C, and there are no known fracture toughness or Charpy impact data on tungsten irradiated at any temperature. Pronounced radiation hardening is observed in W and W-Re alloys irradiated at temperatures of 300°–500°C to doses of ~1–2 dpa, which produces significant embrittlement in tensile tested specimens (~0% total elongation). This radiation hardening is expected to produce a severe reduction in fracture toughness, although experimental measurements of the irradiated fracture toughness are not available. Simple scaling from existing data on irradiated Mo alloys suggests that the operating temperature for W should be maintained above 800°–900°C in order to avoid a significant increase in the DBTT. Whereas tungsten and its alloys are brittle at room temperature, the main engineering design goal is for the material to be ductile under accident conditions and when the reactor is in a “hot shutdown” condition.

Thermal creep, helium embrittlement, or oxide formation issues will determine the upper operating temperature limit for tungsten. The thermal creep of W becomes significant at temperatures above ~1400°C. Helium embrittlement data are not available for tungsten. Based on results obtained on other alloys, helium embrittlement would be expected to become significant at temperatures above ~1600°C (~0.5 melting temperature, T_M). The formation of volatile oxides is a potential problem in tungsten at temperatures above ~800°C. However, if the oxygen partial pressure in the helium coolant can be maintained at or below 1 appm, then the rate of corrosion is calculated to be less than 2 µm/yr for temperatures up to ~1400°C. In summary for this study, the recommended upper temperature limit for tungsten in the structure of helium-cooled systems is ~1400°C depending on the applied stress.

11.2.2 He coolant impurity control — Refractory metals like W, Mo, and V are sensitive to grain boundary oxidation and embrittlement. However, if the oxygen (including H₂O, CO₂, CO...etc.) partial pressure in the helium coolant can be maintained at or below 1 appm, as presented in the last section, then the rate of corrosion should be acceptable temperatures up to ~1400°C. With the use of CCGT as the PCS, as presented in Section 11.7, without the need of using high temperature water in the PCS, the ingress of oxygen impurities should be much lower than the system that uses a high-temperature intermediate heat exchanger (HX) interface with

high temperature and therefore high-pressure water. For impurity extraction from the helium coolant, several powder metal solid getters have been developed. Most are based on Zirconium metal (ZrAl, ZrVFe...etc.). With these materials, hydrogen can be pumped reversibly by temperature control. These solid getters will pump active gases (oxygen, oxides, N, and C_xH_y) irreversibly and have been used on the tokamak experiment TFTR. Recent applications for the semiconductor industry, getters have achieved the control of impurities level lower than 1 appb. These are commercial modular units with no moving parts and are self-monitoring in design. Sandia National Laboratory (SNL) is planning to install a prototype on the helium loop fusion high heat flux testing facility.

11.3 Mechanical Design

The mechanical design of first wall and blanket system in a tokamak reactor has always been very challenging because of the toroidal geometry. Three different first wall and blanket designs for the high-pressure helium coolant design were proposed. These conceptual designs are presented in this section.

11.3.1 basic requirements and assumptions — The mechanical design of the helium-cooled refractory alloy blanket concept must satisfy the basic APEX design goals listed in Table 11.3.1–1. These goals include minimum limits on neutron wall loading, shielding, tritium breeding, and availability as well as provisions for heating and diagnostic penetrations, vacuum pumping, and plasma exhaust around the divertor component.

11.3.1.1. overall configuration — The helium-cooled refractory alloy first wall and blanket concepts developed in the following can be applied to different reactor embodiments and confinement concepts. For the purpose of the mechanical design and maintenance study, however, the ARIES–RS [11.3.1.1–1] reactor configuration was chosen as the basic geometry. Detailed dimensions were selected from the minimum COE and trade off between neutron wall loading and power output. The selected tokamak geometry provides a difficult design challenge but allows direct comparison between the “conventional” first wall and blanket design used for the ARIES–RS study and the high temperature, high power density, helium-cooled refractory alloy blanket concept.

Table 11.3.1–1 First Wall and Blanket General Design Requirements

Function	Requirement	Value/Goal
Power Extraction	Neutron Wall Load Surface Heat Flux Peaking factor	7 MW/m ² average 2 MW/m ² average 1.4
Tritium Breeding	Self Sufficient	TBR > 1
Shielding	Radiation exposure of coils (insulation) Nuclear heating of coils (superconducting cable) Reweldable helium concentration	< 1x10 ⁹ Rad < 1kW/m ³ < 1 appm He
Vacuum	Compatible with plasma – Base partial pressure, nonfuel – Base pressure, fuel (H,D,T)	< 1x10 ⁻⁹ Torr < 1x10 ⁻⁷ Torr
Plasma Exhaust	Divertor required	To remove unburn fuel, helium ash and impurities
Penetrations	Plasma Heating Energy Flux — NBI — RF Diagnostics Pellet Fueling	~4 MW/m ² ~6 MW/ m ² viewing through labyrinth and mirrors penetration
Operation Parameters	Pulse Length Reactor Life Number of startup Disruptions First wall component lifetime	Steady State 30 yr < 30 ≤ 1/yr 15 MW.a/m ²
Availability	Maximize total availability	A _{plant} > 0.75 @ 4 MW/m ² *
Safety	Confinement Boundaries	At least LSA [#] 2

*For neutron wall loading

[#]Level of Safety Assurance 2, large scale passive safety. This means that under accident conditions the reactor can be maintained safe without the need for active measures even when large-scale structures are breached.

In order to meet the intent of the APEX study and adapt the helium-cooled refractory alloy concept, several changes were required to the ARIES–RS design. First, the power density

was increased to obtain the surface heat flux and neutron wall load specified by the APEX preliminary design, presented in Section 11.9. Table 11.3.1.1–1 represents the ARIES–RS and the APEX system code design parameters used for the mechanical design evaluation.

Table 11.3.1.1–1 ARIES–RS and APEX Design Parameters

	ARIES–RS	APEX
Major Radius, m	5.52	5.77
Minor Radius, m	1.38	1.44
Plasma Aspect Ratio	4	4
Fusion power, MW	2171	3372
Neutron Power, MW	1736	2698
Plasma power density, MW/m ³	6.38	8.565
Number of Sectors	16	16
Outboard:		
Average neutron load, MW/m ²	4.03	5.35
Peak neutron load MW/m ²	5.67	7.49
Ave. first wall surface heat flux (radiative), MW/m ²	0.4	1.55
Peak first wall surface heat flux, MW/m ²	0.47	2.16

In order to accommodate the helium-cooled refractory alloy blanket few changes are required in the ARIES–RS configuration. The double-null divertor is maintained, as is the segmentation of the blanket poloidally. The blanket is integrated into a single unit per machine sector, where a sector is one-sixteenth of the machine. Figure 11.3.1.1–1 shows a comparison of the ARIES–RS and the modified configuration for the APEX helium-cooled refractory alloy concept.

11.3.2 blanket module design — Since helium-cooled blankets have been proposed in the past, the APEX helium-cooled concept represents an evolutionary design. Several helium-cooled designs are described in the BCSS study [11.3.2–1] and a helium-cooled blanket/shield system was proposed for ITER in 1993 [11.3.2–2]. The primary difference between the earlier studies and the present study is the use of refractory alloy material that allows higher temperature operation and higher performance of the APEX design.

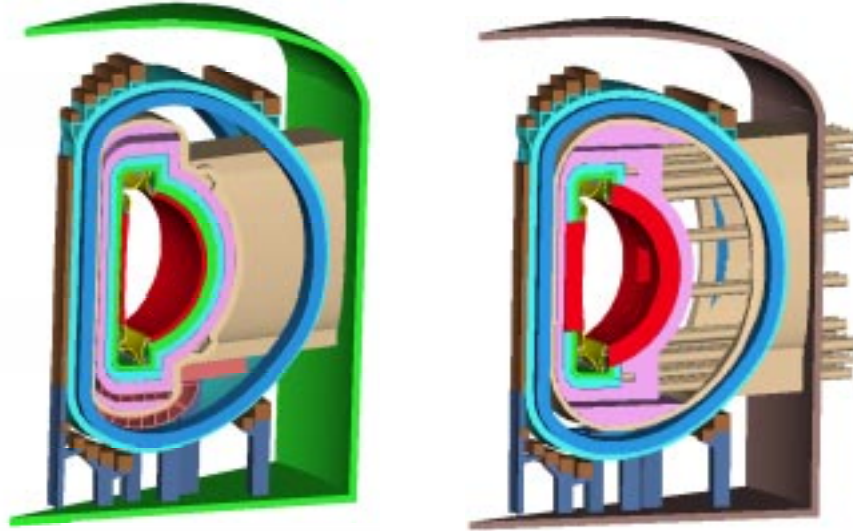


Fig. 11.3.1.1-1 Comparison of ARIES-RS and APEX configuration.

The helium-cooled refractory alloy concept for APEX replaces the conventional first wall, blanket, and high temperature shield of the ARIES-RS design with a set of integrated modules that include a high temperature helium-cooled first wall and a lithium bath that is also cooled with high temperature helium. The mechanical design of the module must incorporate a first wall structure, a lithium bath structure for breeding and shielding, helium tubes for removing the nuclear heating from the lithium bath and surrounding structure, manifolds for distributing the helium and a back structure for supporting the blanket. Desirable design features include:

- Discrete modules attached to structure/manifold assembly
- Minimum void space for better shielding
- Maximized double containment
- Welds inside lithium bath and behind first wall and blanket
- Common plenum for lithium allows pressure relief for leaks
- Strong back module configuration to minimize volume fraction of structural material in front of the first wall and blanket
- Near constant temperature structure to minimize thermal stress
- Apply configuration that can further minimize thermal stress

When compared with conventional structural materials, the last two features are relatively more important to the W-alloy because of the project significant embrittlement under low neutron fluence as described in Section 11.2 and Chapter 13.

The APEX helium-cooled refractory alloy mechanical design has undergone three revisions. The basic parameters of the three design versions are listed in Table 11.3.2–1. The primary difference in the three versions is the helium operating temperature. In the first two concepts, the modules are small units and every effort was made to minimize the problems associated with the large temperature rise in the helium. The first version, shown in Fig. 11.3.2–1, incorporates a large number of modules (10 outboard modules per sector in the toroidal direction and 9 in the poloidal direction). The units themselves consist of a lithium filled can with numerous helium-cooling loops serpentine within the can. The loops provide large surface area with a minimum number of connections. A plenum at the back of the can is intended to double-contain all the helium connections that are internal to the module. However, this concept requires a significant number of external manifold connections that are not double contained. The first wall is a separate unit that is structurally separated from the module except at

Table 11.3.2–1 APEX Helium-Cooled Refractory Alloy Concept Parameters

	Version 1 & 2	Version 3
Coolant		
– He inlet temperature	400°C	800°C
– He outlet temperature	1000°C	1100°C
– He pressure	8 MPa	120 MPa
Materials		
– Blanket, tube, shell material	Vanadium and Tantalum	Tungsten
– First Wall material	Tungsten	Tungsten
Configuration		
– First Wall	Formed tubes, toroidal flow	
– Blanket and shield	Nested coolant tubes in lithium bath, toroidal flow	
Inboard		
Number of module	4 for version 2	2
Midplane module width (m)		
Outboard		
Number of module	6 for version 2	3

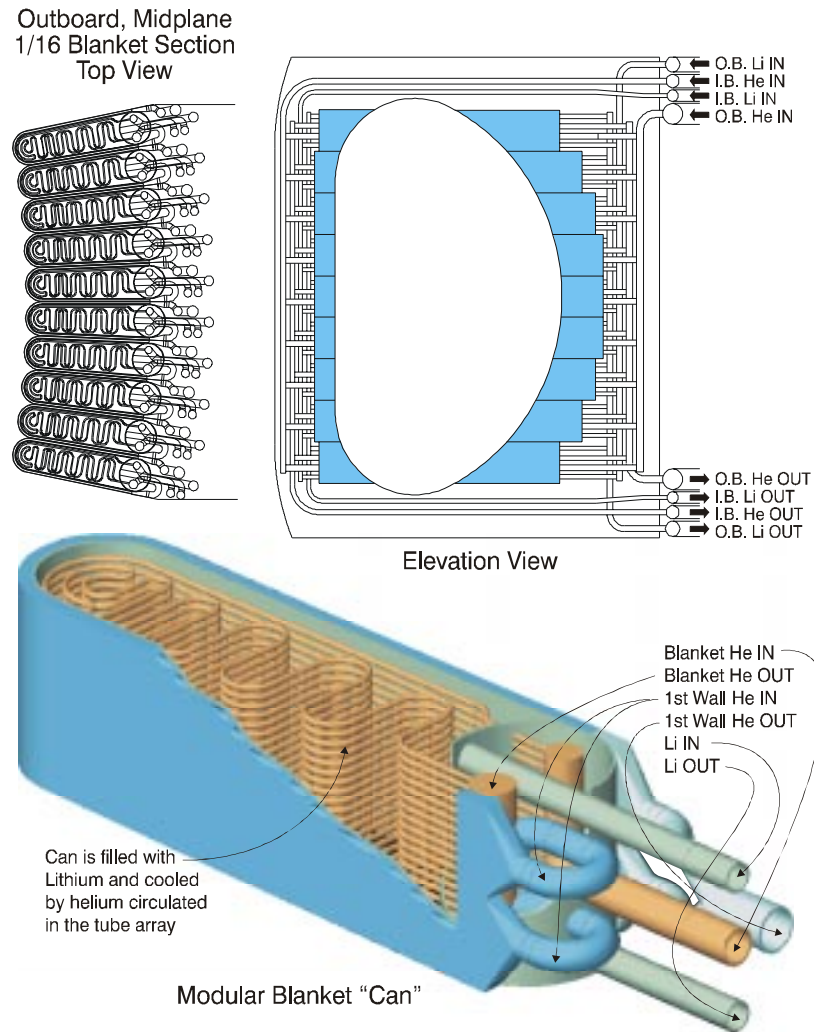


Fig. 11.3.2-1 Schematic of Version 1 design.

the piping connections in order to accommodate relative thermal expansion between the module and first wall. The first wall is in series with the inlet and exit pipes from the blanket module. Helium enters the blanket manifold at 400°C, is routed through the module and into the first wall at about 900°C, and exits the first wall at 1000°C.

The next version is shown in Figs. 11.3.2-2 through 11.3.2-4. This concept attempted to solve several problems not addressed in the first concept. First, the number of modules in the toroidal direction has been reduced to four inboard and six outboard. Second, there are no helium connections in vacuum except for the first wall connections. Third, the lithium volume of each module is connected through the backplate structure to provide pressure relief in the event of a large leak inside the lithium. Finally, the helium manifolds are coaxial with slip joints in the return pipes. This provides a means to keep the entire structure at the temperature of the lithium bath, while allowing the helium manifolds and internal heat exchange tubes to operate at the

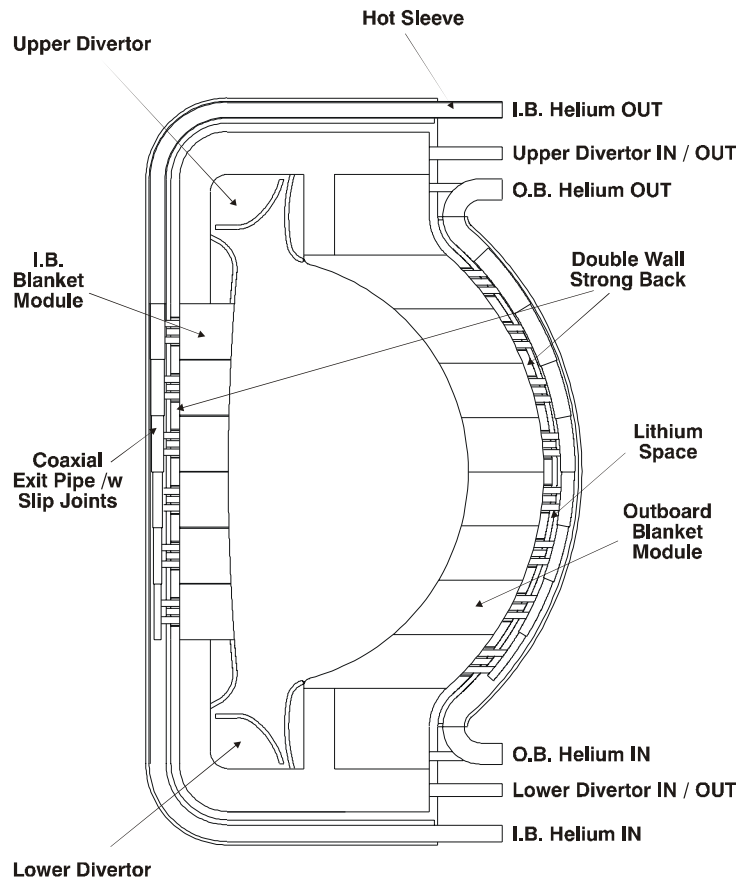
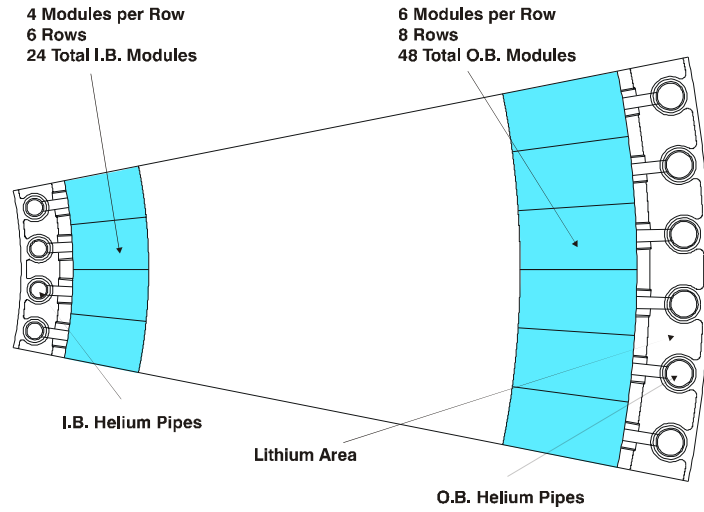


Fig. 11.3.2-2 Version 2 plan and elevation view.

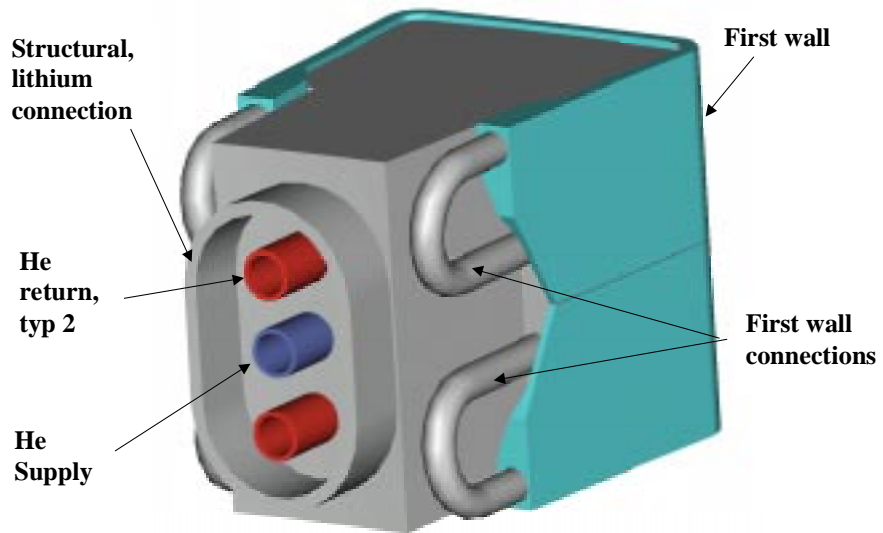
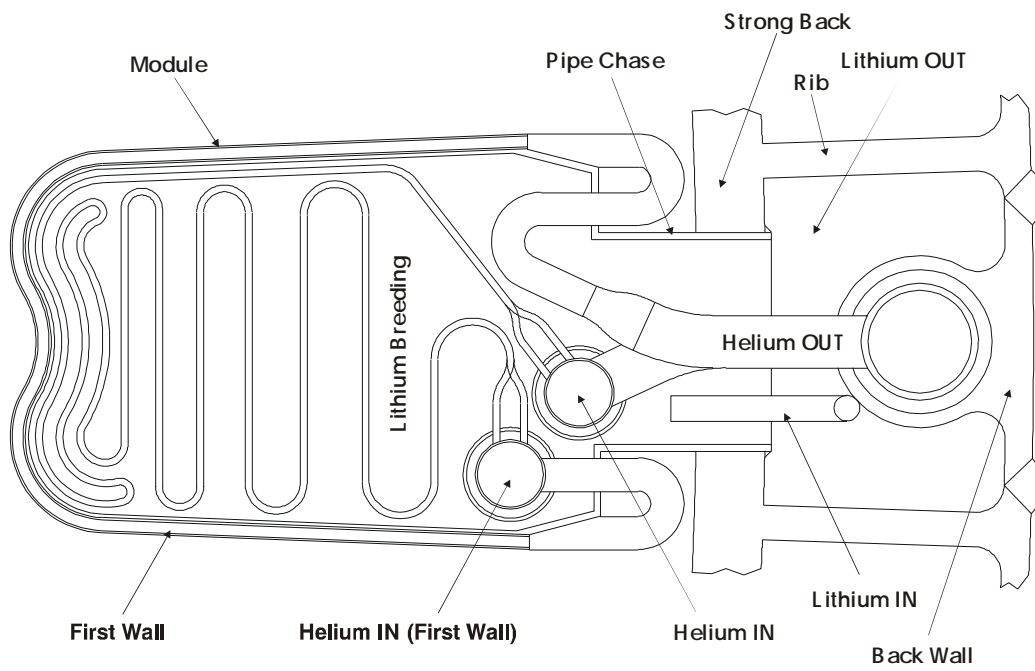


Fig. 11.3.2-3 Version 2 module details.

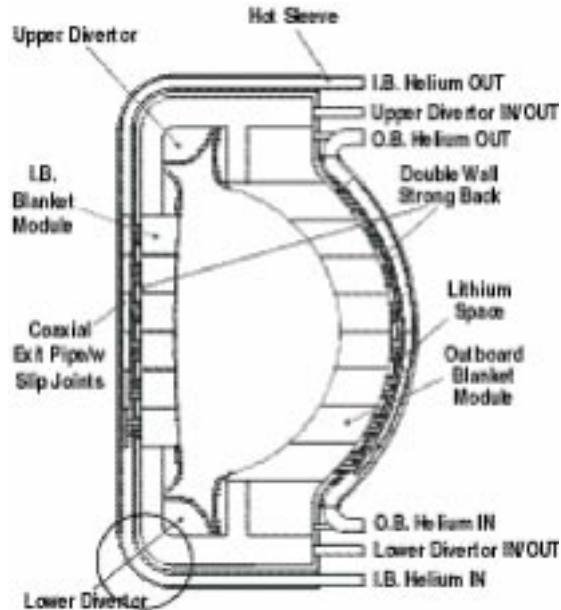


Fig. 11.3.2-4 Version 2 coaxial manifold and module connection details.

temperature extremes. Since all the helium flows from top to bottom, the coaxial pipe is tapered from a large, low temperature supply pipe and smaller high temperature return at the bottom to a large return and smaller supply pipe at the top. This allows the helium fraction (corresponding to a void in the shielding) to be constant from top to bottom. To avoid thermal stresses, each section of the return pipe is connected to a single module, such that the pipes can expand in either direction by sliding on the mating sections of the return pipes. Since the return pipe is completely enclosed by the supply pipe, there is no need for a hard seal. The leakage between the supply and return manifolds should be minimal although care must be taken to avoid diffusion bonding of the sliding surfaces. The piping arrangement is the same as the first version with the helium entering the module at 400°C and exiting the first wall at 1000°C.

The third version is shown in Figs. 11.3.2-5 and 11.3.2-6. This is a more conservative approach avoiding the coaxial slip joints in the return pipes. But the module structural support with the accommodation of coolant inlet and outlet temperature gradient will be much more difficult. A gradual vertical structural support connected to the VV while allowing graded deflection to accommodate the dimension change is proposed. In this design, the temperature difference between modules has been reduced from 700° to 300°C. This provides a chance to reduce the number of modules to a single unit in the poloidal direction, except at penetrations, and the relaxation of the thermal stresses induced by the temperature differential. There are two inboard and three outboard modules per sector in the toroidal direction.

The large modules contain the lithium in a single volume with lithium in the breeding zone and a combination of lithium and steel balls in the shielding zone. The temperature is relatively uniform, although there will be some gradients, albeit transient, between the front and back structural walls.

Helium Cooled Blanket Concept One of three "cans" per outboard sector shown with top removed

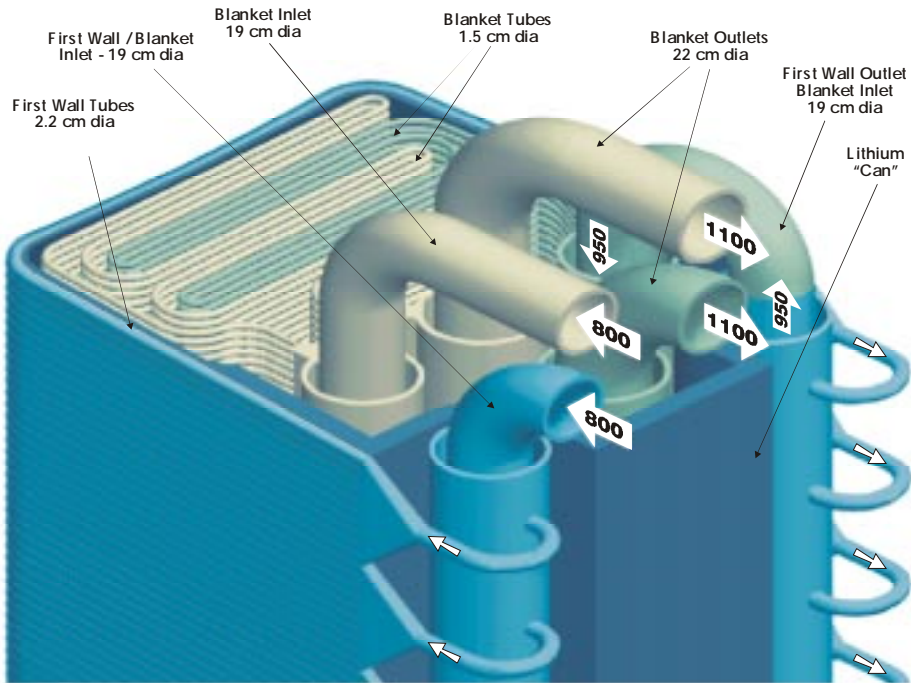


Fig. 11.3.2-5 Version 3, large module design 3-D view near top of outboard module.

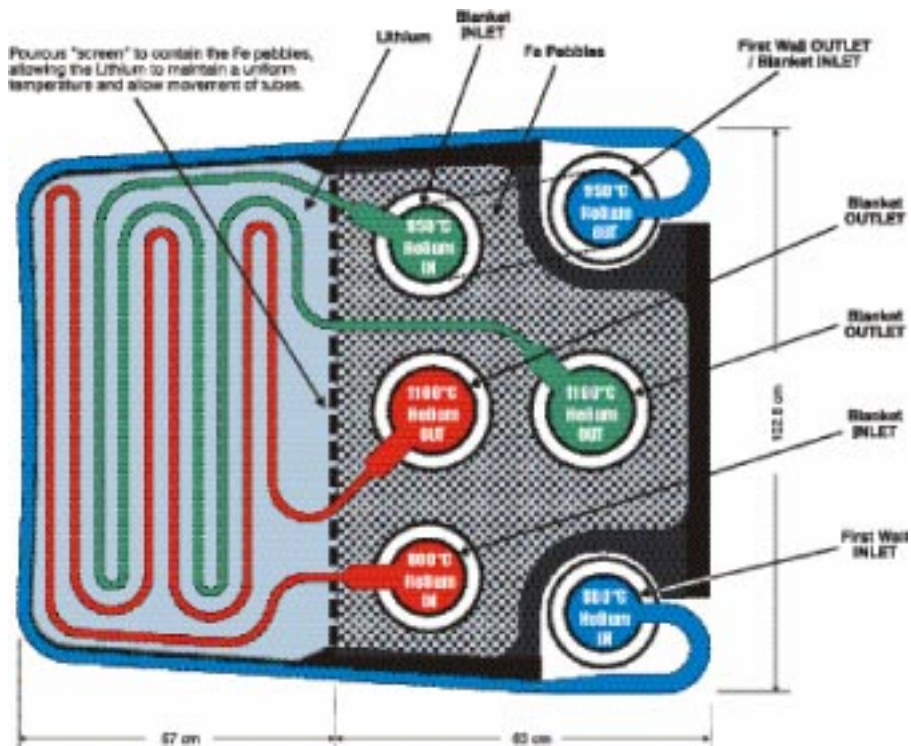


Fig. 11.3.2-6 Version 3, plan section through outboard module.

As in the other designs, the first wall is made up of individual tubes grouped into separate units which in this case are connected to separate cooling manifolds at the back of each module. The first wall units consist of multiple parallel passages connected through an integral manifold to round inlet and outlet connections. The round connections should be easier to fit up and minimize thermal stresses at the interface.

The piping is routed in two circuits. The first circuit includes the first wall and part of the interior heat exchange tubing. Helium at 800°C enters the first wall through the supply manifold and exits into the first wall outlet manifold at 950°C. The helium is then routed inside the lithium can to the first supply manifold for the tubes. The first tube circuit exits into a return manifold at 1100°C and is directed through the large midplane ports to the outside of the machine. The second tube circuit is fed at 800°C and exits at 1100°C. A schematic of the cooling system is shown in Fig. 11.3.2–7.

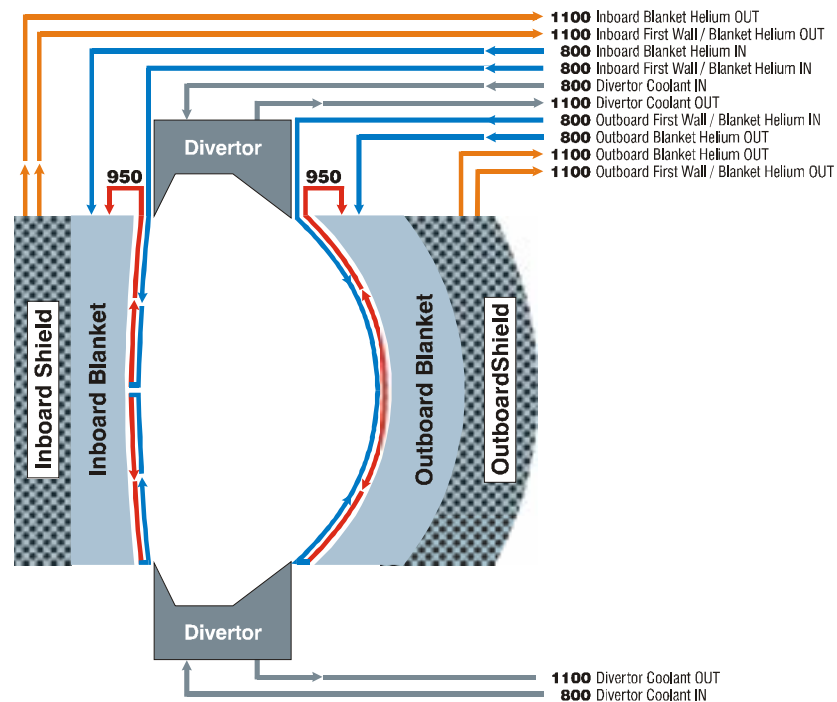


Fig. 11.3.2–7 Version 3 flow/temperature schematic.

11.3.3 maintenance approach — One of the primary goals of the APEX study is to increase the availability of fusion reactors by increasing the mean time between failures and by decreasing the mean time to repair. To this end, the helium-cooled refractory alloy preliminary design point focused on the following goals:

1. Modular maintenance for everything, with increased ease of access for high risk and high damage components.
2. Avoid maintenance inside machine, if at all possible.

3. Use of pretested modules for all components, with minimum field welding of high-pressure joints.
4. Protect the VV and coil set, as these are lifetime components.

The first and second goals, modular maintenance using pretested components, are achieved by providing cassette-type maintenance within a single sector module. The high maintenance items, including the divertor and heating/diagnostics are contained in separately removable cassettes. The rest of the blanket/shield system is part of a sector module that can be removed as a single unit for major maintenance. The time to replace a single divertor sector or diagnostic cassette is presumed to be significantly less than the time to replace an entire blanket sector. Both replacement times are less than deployment of in-vessel maintenance equipment which requires those repairs to be done *in situ*. The possibility of welding of refractory alloy materials *in situ* is not known. Pretesting of the cassettes and sector assemblies is possible and necessary for improving reliability.

The third goal is important, since it is imperative to protect the VV, which is the primary safety barrier. In the helium-cooled refractory alloy design, the sector module contains all the shielding necessary to protect the vacuum/safety barrier to damage levels below the rewelding limit for the vessel of 1 appm. If the VV must be breached to maintain coils, it is prudent that it can be a local repair and not require the full replacement of the vessel. It is also prudent to limit structural damage to allow use of nonirradiated properties for design, since it would certainly complicate the design, licensing, and maintenance by allowing the first safety barrier to degrade during operation.

11.4 Blanket Thermal-Hydraulics Design and Analysis

The use of helium as a first wall coolant has been proposed in various fusion design studies. For example, an analysis of the effectiveness of heat transfer enhancers such as surface roughening and fins was done for a helium-cooled divertor option for ITER [11.4–1]. Helium cooling is also used in the ARIES design study [11.4–2]. The main difference in the current work is the high helium outlet temperature (950°C) of the first wall. In order to have a consistent first wall and blanket design, we performed design iteration between the areas of mechanical, thermal-hydraulics, and nuclear design. This section reports the result of the thermal-hydraulics evaluation of the helium-cooled refractory alloy first wall and blanket designs.

11.4.1 design inputs — With the mechanical design concept described in Section 11.3 and the volumetric power generation projected from nuclear analysis, we performed thermal-hydraulics analysis to determine the material volume fractions of the first wall and blanket zones of mechanical design Version 3. The material volume fractions were then used for the next iteration of nuclear analysis. For this calculation, the normalized volumetric power density for W-alloy as a function of distance x , in mks units, from the first wall is approximated by, $PW(x) = 9e^{-3x}$ MW/m³, per neutron wall loading in MW/m². The normalized volumetric power density for Li-breeder is approximated by $PLi(x) = 4e^{-3x}$ MW/m³. Other input parameters are listed in Table 11.4.1–1.

Table 11.4.1–1 First Wall and Blanket Design Input Parameters

Reactor power output, MWe	2005
Reactor thermal power, MW	3975
Helium pressure, MPa	12
Helium mass flow-rate, kg/s	2528
Helium T_{in}/T_{out} , °C/°C	800/1100
Structural material	W-5Re
Max. neutron wall loading, MW/m ²	7.49
Max. surface heat flux, MW/m ²	2.16
Total first wall area, m ²	483
Number of first wall sectors	48
First wall sector area, m ²	10
Midplane sector width, w, m	0.94
Sector height, m	6.1

As noted in Table 11.4.1–1, the maximum neutron wall loading is lower than the APEX maximum designing goal of 9.8 MW/m². This lower value of 7.49 MW/m² actually corresponds to the minimum COE at a power output of 2 GWe as obtained from system study presented in Section 11.10.

11.4.2 first wall design with he-cooled porous medium — The goal in designing a refractory alloy helium-cooled first wall is to develop a robust design that can withstand a surface heat load of 2 MW/m² or greater with a coolant pressure of 12 MPa and first wall outlet temperature of 900° to 950°C. Higher gas pressures which also means higher mass density can be used to improve heat transfer or reduce the coolant system pressure drop and, therefore, increase the thermal efficiency of the CCGT power conversation system. The design objective is also to minimize the thermal stresses and the total stress in the first wall.

The input design parameters are given in Table 11.4.2–1. These parameters and the design objective set the basic dimensions of the first wall cooling passages and flow conditions. We used a round tube to minimize the primary stress from coolant pressure. For a thick-walled coolant channel of outer radius r_0 and inner radius of r_i , the differences between the radial and tangential stresses, $(\sigma_r - \sigma_t)$ which is the quantity that determined yield, is given by $\sigma_r \max - \sigma_t$

Table 11.4.2–1 He Flow Parameters

Outer radius, r_0 , mm	11	8.5
Inner radius, r_i , mm	8	5.5
Area fraction of open porosity, f_{porous} , %	90	90
Porous medium flow area, $\pi f_{\text{porous}} r_i^2$, mm ²	181	85.5
Unit heat load, $Q_{\text{unit}}=Q_{\text{FWS}}/2\pi r_0$, MW	42.808	33.079
Temperature rise in first wall, T_{rise} , °C	100	100
Heat capacity, C_p , J/kg-K	5192.6	5192.6
Density, ρ for He @ 900°C and 12 Mpa, kg/m ³	4.925	4.925
Mass flow per channel, $\dot{m} = Q_{\text{unit}}/(C_p T_{\text{rise}})$, kg/s	0.082	0.064
Mass velocity, kg/m ² s	455.6	744.8
Velocity, v , assuming 90% open porosity, m/s	92.5	151.2

$\sigma_r \max = p \frac{r_i^2}{r_0^2 - r_i^2}$. [From Popov Mechanics of Materials (Justice-Hall, 2nd Ed.) the maximum

stresses for an internally pressurized thick-walled cylinder are: $\sigma_r = \frac{pr_i^2}{r_0^2 - r_i^2}$, $\sigma_r \max = \frac{pr_i^2}{r_0^2 - r_i^2}$

$\left(1 - \frac{r_0^2}{r_i^2}\right)$, $\sigma_t = \frac{pr_i^2}{r_0^2 - r_i^2} \left(1 + \frac{r_0^2}{r_i^2}\right)$, $\sigma_t \max = \frac{pr_i^2}{r_0^2 - r_i^2} \left(1 + \frac{r_0^2}{r_i^2}\right)$ $\sigma_t \max - \sigma_r \max = p \frac{r_i^2}{r_0^2 - r_i^2}$. The yield

condition is given by $Y = \sigma_t \max - \sigma_r \max = \frac{pr_i^2}{r_0^2 - r_i^2}$.] If we fix the inner radius and let r_0 and the

wall thickness ($r_0 - r_i$) vary, the differential stress ($\sigma_r - \sigma_t$) decreases rapidly with wall thickness and is only significant compared to the anticipated thermal stresses for relatively thin walls (<1.5 mm) that are not considered acceptable for APEX. For noncircular channels, local stresses, near features such as internal angles, due to the pressure would be much higher.

A greater challenge is dealing with the thermal stresses, which increase with the wall thickness. The thermal stress in a constrained plate with a thermal gradient dT/dx , is given by $\sigma_{\text{thermal}} = \alpha \frac{dT}{dx} t_{\text{wall}} \frac{E}{1-2\nu}$. For tungsten as the material and a surface heat load of 2 MW/m², the thermal stress in this case is about 74 MPa per mm of wall thickness.

Figure 11.4.2–1 compares the pressure and thermal stresses as a function of wall thickness for tungsten at ~1000°C (materials properties), an outer channel radius of 9 mm and a surface heat flux of 2 MW/m². The thermal stresses far exceed the pressure stresses except for small values of the wall thickness. However, based on the constrained plate model, these thermal stresses are unacceptably high and the main objective in the first wall design is to mitigate these

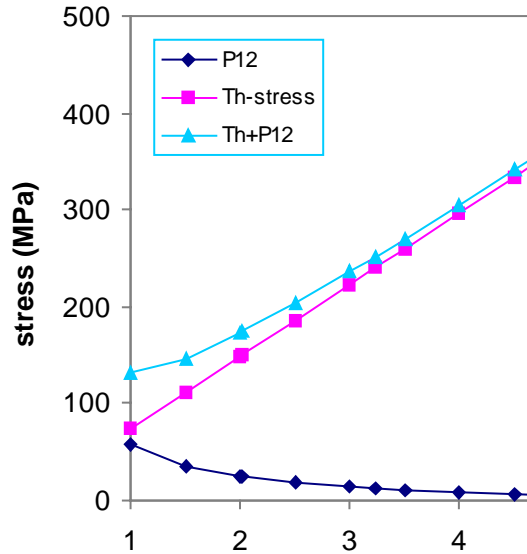


Fig. 11.4.2-1 Thermal stress in first wall based on the constrained plate model.

high thermal stresses. This is a conservative estimate. Compare to a thin wall circular tube estimate the thermal stress will be lower by a factor of $(1 - 2\nu)/2(1 - \nu) = 0.32$. Therefore, results based on the constrained model and thin wall circular tube model will give us a simple estimate on the thermal stress of the first wall design. In the following, we will continue our analysis based on the conservative constrained plate approximation.

Let us take a basic design point with a coolant passage of 8 mm radius and a wall thickness of 3 mm. These values and the information below now specify the flow conditions.

11.4.3 porous medium first wall design — The design activity reported here built in part upon development activities by two small businesses was incorporated into the design of the helium-cooled first wall. The first was the use of a porous medium to enhance heat transfer. Thermacore, Inc., designed and built a series of helium-cooled modules that were tested at SNL and elsewhere. Second was experience in fabrication of refractory materials by Ultramet, Inc. Ultramet has designed and built commercial products made of refractory metals for rocket nozzles and other applications in which Ultramet uses a metallized foam that is integrally bonded to fully dense material.

Thermacore, Inc. of Lancaster, Pennsylvania, through grants from DOE’s Small Business Innovative Research (SBIR) Program, developed water-cooled and helium-cooled modules that utilized brazed copper balls as a porous heat transfer medium in copper, Glidcop™ or molybdenum coolant channels.

Their objective was easy-to-fabricate designs for heat sinks that operated at moderate temperature. The specific applications were (1) Faraday shields for DIII-D, and (2) a mockup for a divertor module for ITER [11.4.3-1,11.4.3-2].

The helium-cooled Faraday shield had a molybdenum outer skin with copper ball-aggregate for the porous medium. One advance in their development of a helium-cooled heat sinks was the development of designs that connected open axial inlet and exhaust passages to circumferential flow passages that contained the porous medium (see Fig. 11.4.3-1). With this configuration, helium flows only a short length (half the circumference) through the porous medium. This reduces the pressure drop as compared with axial flow through channels filled with the porous medium. Recent test results are to be reported in ISFNT-5 [11.4.3-3].

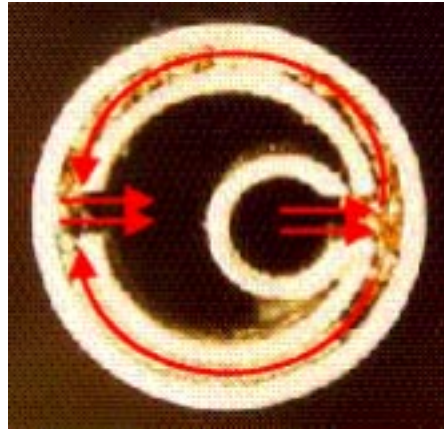


Fig. 11.4.3-1 Thermacore circumferential flow design.

11.4.3.1 materials — The generic designation of tungsten has been satisfactory thus far in the design as the selected material since the basic and essential information for analysis (thermal properties and elastic modulus) apply to many tungsten alloys as well as pure recrystallized tungsten. Others issues such as radiation resistance, ductility and yield strength that are certainly important affect whether the resulting stress levels are acceptable but do not affect the actual execution of the thermal analysis. These materials issues and data on properties and performance are discussed in Section 11.2 and Chapter 13 of this report.

A conservative approach in this work was to keep the operating secondary stresses below ~75 MPa. This is well within the guidance given by the APEX Materials Group, following the ASME design criteria of primary design criteria $S_m \leq 1/3$ ultimate stress or $2/3$ yield stress, whichever is lower of the material at temperature for ductile material. For the secondary stress = (primary + bending + thermal stresses), it should be lower than $3S_m$. Figure 11.4.3.1-1 shows a recent compilation of estimated allowable design stresses (S_m) for various tungsten products. This criteria will be revised when more irradiated data for W-alloy is available due to the loss of ductility under low neutron fluence.

As may be seen from this figure, for tungsten alloys at working temperatures below ~1100°C the value of 75 MPa is acceptable including W-5Re.

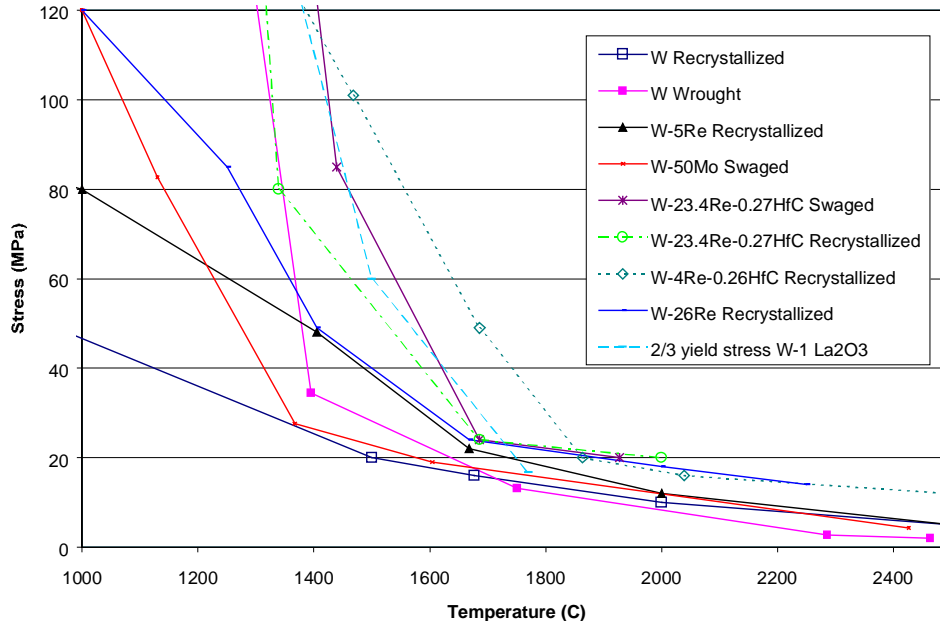


Fig. 11.4.3.1-1 Design stresses (S_m) for tungsten and tungsten alloys.

A secondary objective in this work was to use the evaluations of performance of the helium-cooled first wall design to assess what capability there may be for surface heat loads beyond 2 MW/m^2 . Higher allowable stresses and higher ceiling temperatures are clearly possible based upon the information in Figure 11.4.3.1-1. The capability to handle significantly higher heat loads might indicate the potential for applications of a He-cooled module for divertor heat sinks or baffles or for first walls in higher power density devices. Increasing the performance of tungsten alloys is discussed in the materials sections of this report (Chapter 13). A note is added here to document a planned collaboration in this area being carried out under the auspices of the US-Japan Bilateral Agreement. Prof. Hiroaki Kurishita of the Institute for Materials Research at the Oarai Branch of Tohoku University has studied the effects of modifying W or Mo with “nanodispersoids” (TiC or HfC, 10 nm fine, 200 nm coarse) to achieve fine grain size (1–12 microns) [11.4.3.1-1 through 11.4.3.1-3]. Potential benefits are improved ductility and resistance to embrittlement from irradiation. However, notched samples or HHF mockups have not yet been tested. In July 1999, SNL will host Prof. Hiroaki Kurishita as part of a US-Japan collaboration. His nanodispersion tungsten will be used to make samples for notched-bending tests and armor for a high heat flux mockup that will be tested at SNL.

11.4.3.2 fabrication — The initial effort on a design for a helium-cooled first wall followed the design by Thermacore and simply substituted tungsten (W) as the material. The primary drawback was in fabrication. Thermacore had brazed their structures. This was not likely to be satisfactory for the high temperature application desired.

The concept for the both the porous medium and the fabrication were revised after discussions with Ultramet of Pacoima, California. Ultramet uses a process in which they build up refractory material with chemical vapor deposition (CVD).

Figure 11.4.3.2-1 shows a Ta foam with 80 pores/in., 15% density, and an outer circumference with a machined thread. The precursor is then pyrolyzed in place to give a rigid graphite structure that is subsequently coated with metal or ceramic material in a CVD process [11.4.3.2-1]. The item is used for bone implants.

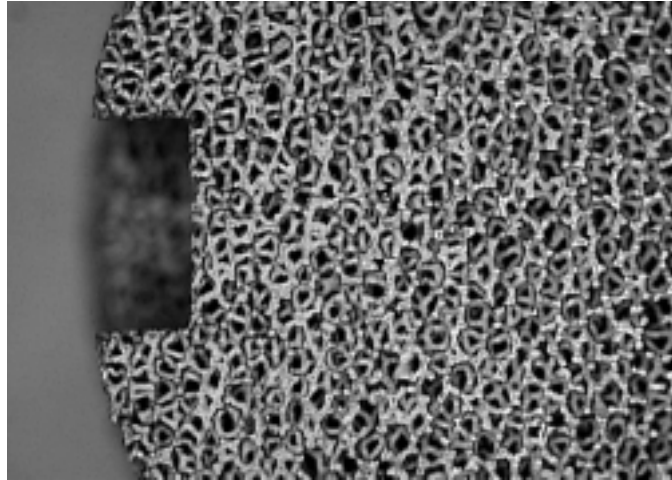


Fig. 11.4.3.2-1 Porous Ta implant, diam. is 0.75 in.

To obtain metal foam with high open porosity, they begin with a plastic foam precursor that is cut to the desired shape. In Fig. 11.4.3.2-2 is a HX with an Inconel 718 outer shell, a Re liner and Re foam on a 0.75 in. ID Mo mandrel.



Fig. 11.4.3.2-2 Ultramet Re foam, HX.

The Re foam is 15% dense with 45 pores/inch. Ultramet indicated that the foam could initially be squeezed in two dimensions to give elongated pores as small as ~0.05 mm diameter.

The cell shape is more evident in the previous figure. Irregular ligaments rather than 2-D walls make up the structure.

The high amount of open porosity and the limited surface area both offer promise for significantly reducing the pressure drop along the flow path compared with the ball-aggregate concept. The initial intent in developing the refractory alloy He-cooled first wall was that the open porosity of the metallized structure would have a low enough pressure drop for axial flow in a channel filled with metallized foam. In principle, a design that combined the metallized foam fabrication technology with the circumferential flow concept also seems possible and would have the advantage of reducing the axial pressure gradient along the first wall at the cost of a somewhat more complex internal configuration.

11.4.3.3 high heat flux testing of He-cooled modules — In addition to design studies, hardware development of helium-cooled plasma facing components has continued in the fusion program. Helium-cooled test modules of several types have been tested in the Electron Beam Test System (EBTS) at the Plasma Materials Test Facility operated by SNL as shown in Table 11.4.3.3–1. A divertor mockup made by Thermacore and tested in 1998 withstood steady-state heat fluxes above 35 MW/m² in tests in EBTS in which the heated spot was much smaller than surface of the module. However, the results are somewhat misleading in that they are not representative of the much lower values of maximum steady-state heat flux that are obtained when the entire surface of a helium-cooled heat sink is heated. The ultimate performance of this

Table 11.4.3.3–1 SNL High Heat Flux Tests in Helium-Cooled Test Articles

Year	Type of Test Article	Fabricator
1993	Microchannel HX (~100μ channel size)	Creare, Inc.
	Divertor mockup A (0.46 mm channels)	General Atomics
	Porous metal HX (40% porosity, 0.43 mm diam.)	Thermacore, Inc.
1994	Dual channel porous metal HX	Thermacore, Inc.
	Divertor mockup A retest at higher heat loads	General Atomics
1996	Phase-II porous metal HX	Creare, Inc.
	Vanadium HX	General Atomics
1997	Faraday shield A	Thermacore, Inc.
	Divertor mockup B	Thermacore, Inc.
1998	Faraday 2 nd shield B	Thermacore, Inc.
	Divertor 2 nd mockup C	Thermacore, Inc.
1999	Divertor mockup B retest, added diagnostics	Thermacore, Inc.

heat sink with a uniform heat flux over its entire surface cannot be evaluated at present because the heat load exceeds the heat rejection capability of the helium loop currently in EBTS.

Figure 11.4.3.3–1 shows the He-cooled divertor mockup made by Thermacore, Inc. Additional instrumentation was recently added to this module so that the effects of bypass flow, *i.e.*, flow instabilities and decrease in performance when only one of two parallel channels is heated [11.4.3–3].

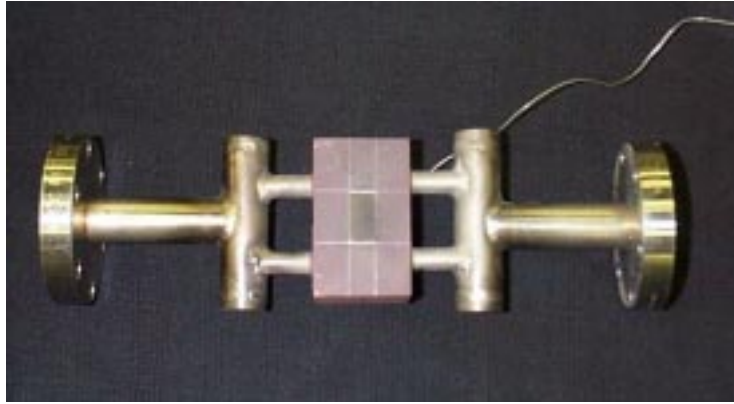


Fig. 11.4.3.3–1 Thermacore He-cooled test module.

11.4.3.4 design approach — A “ground rule” of the APEX study was that structures should be robust and, specifically, that the designers should not resort to thin first walls (*e.g.*, >2 mm) to relieve the thermal stresses. Thus, 3 mm was taken as a nominal wall thickness. (In mechanical design, with coolant passages of radii less than 10 mm, this is a “thick-walled design” even for containing a coolant pressure of 8–12 MPa.)

A central challenge in the design is somehow to relieve the primary bending strain that results from the high surface heat load and the related steep thermal gradient in the heated surface. An extended surface area to enhance heat transfer was considered a desirable feature.

A challenge with regard to fabrication is the objective that the first wall, including any extended area for heat transfer such as a porous medium or fins, should be an integral structure rather than, for example, having a brazed or welded (if this were possible) joint. There should be no joints in the first wall channels.

The design utilizes the following basic approaches to solving the challenges noted above. A porous medium enhances heat transfer from the wall to the helium. This enhances the heat transfer and thereby reduces the temperature drop from the wall to the helium and the absolute temperatures in the heated part of the first wall. Also, the design employs the technique of “tailoring” the heat transfer coefficient locally for reasons described below. The “tailoring” would reduce heat transfer by using a thermal barrier or, more simply, by not attaching the porous medium in these areas.

To reduce the thermal stresses in the first wall during operation, the first wall is not constrained against bending; outward bowing of the first wall toward the plasma is permitted along the length of the first wall. Also, the heat transfer around the perimeter of the cooling passage is “tailored” to reduce heat transfer in areas like the sidewalls and web. The objective of

this tailoring is to obtain, as near as possible, a linear gradient in temperature through the thickness of the cooling channel and thereby minimize the thermal stresses. With bowing of the first wall allowed, it is only the deviations due to a nonlinear temperature gradient through the thickness of the channel and the stresses associated with the coolant pressure that remain. (The bowing of the channel relieves a linear stress pattern through the thickness of the channel; this pattern would otherwise be the primary bending stresses associated with the heat load.)

11.4.3.5 thermal analysis — The primary tool in developing the design of the porous first wall was thermal analysis of 2-D models. Models were developed and modified to evaluate the effects of the following features: several values of the surface heat flux and of the internal pressure, changes in the overall shape and features, such as the web thickness in the configuration with dual coolant passages, and modifications to the heat transfer coefficients around the perimeters of the coolant passages.

The model geometry was generated in PATRAN and then analyzed in ABAQUS. Typically, the models contained about 1000 elements and used a 4-noded quad element (DC2D4) for heat transfer and a 6-noded element (CGPE6) for stress analysis with generalized plane strain.

A thermal treatment for the porous medium was not incorporated in the models. In this regard the solutions are not self consistent. Instead the heat transfer was handled simply by specifying the heat transfer coefficient locally at the boundary and setting a uniform sink (coolant) temperature. (A self consistent solution with the heat transfer in the porous medium properly treated is clearly a desirable goal both because the accuracy of the model would be improved and because this is an interesting problem. However, greater priority was given to a simpler approach that could be used to assess the effects of changing the heat transfer coefficient locally around the perimeter of the coolant passage. The justification is two-fold. First, the simpler approach does permit the necessary evaluation. Second, the assumption is probably not a bad one since the primary heat transfer surfaces at the front and at the back of the channel are well separated and in each area the lateral temperature variations are not large, so the main heat conduction is essentially 1-D into the helium. Also, one can argue that if the results of “tailoring” give the anticipated benefit, then the main point is proven and discrepancies between a self consistent model and the approximations here would be handled by revising the prescribed.)

Figure 11.4.3.5–1 shows the layout of the last model (HeE) and is a stress map of the von Mises stress with the distortion greatly magnified (elastic displacements X1000) for a surface heat load of 2 MW/m^2 and an internal pressure of 10 Mpa and at 1000°C . The maximum von Mises stress is $\sim 80 \text{ MPa}$. Table 11.4.3.5–1 shows some sample data from the thermal analysis.

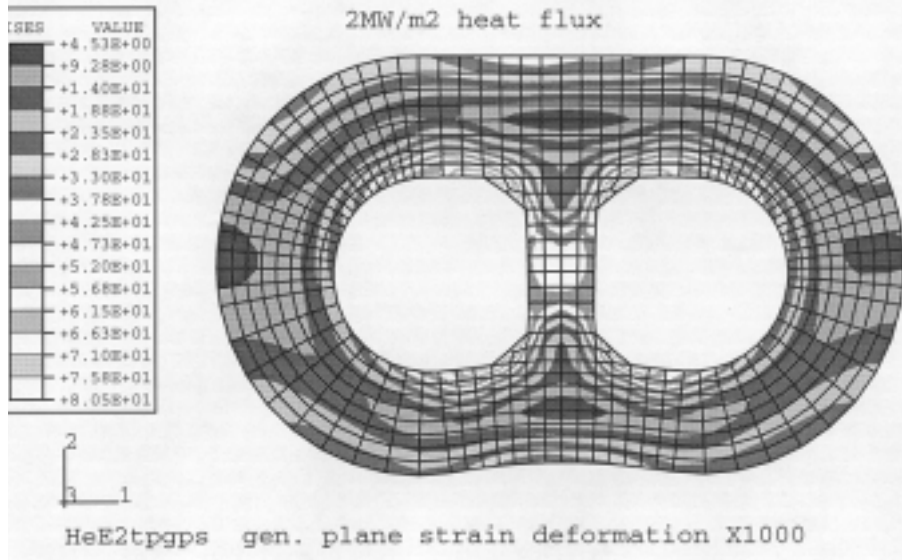


Fig. 11.4.3.5-1 Model configuration used for 2-D thermal analysis.

Table 11.4.3.5-1 Stresses from HeE Model Output

Model:	HeE2gps	HeE2tbgps	HeE4gps	HeE4tbgps
Q_{FW} (MW/m ²)	2	2	4	4
S11 ^(a) (MPa)	81.5	78.8	125.4	106.5
S22 ^(a) (MPa)	41.7	44.4	51.2	44.7
S33 ^(a) (MPa)	62.7	62.3	101.4	77.6
Von Mises	79.1	78.2	104.5	96.8

^(a)The stresses (S11,..) are maximum values and are not at the same location.

The designation “tb” within the names in Table 11.4.3.5-1 (*e.g.*, HeE2tbgps) means that in these cases the heat transfer coefficient, h , was locally modified along the perimeter. Specifically, there was no direct heat transfer to the helium ($h = 0$) along the lower portion of the sidewalls and the sides of the center web; h was set equal to 20,000 W/m²-K elsewhere.

In the earlier work, simple rectangular models were evaluated initially then the dual channel configuration was chosen. With the dual channel, if coolant flow is reduced in one passage, there can still be significant cooling if helium flow continues in the other channel. This is perceived as an advantage for safe shutdown in the case where some retardation of flow is observed. However, at this point there is not sufficient analysis to prove this assumption.

As the configuration for the design was developed, the thermal stresses were somewhat reduced by modifying the shape of the first wall tubes; however, there is still room for

improvement in this regard. The maximum von Mises coolant stress is ~28 MPa, at corners of the inner web, for P_{coolant} of 10 MPa and might be reduced further.

The success of the design in mitigating the thermal stress in the first wall can be measured in part by comparing the stresses of the model (HeE) to those in a simple beam or constrained pipe with the gradient in temperature from a surface heat load of 2 MW/m².

Figure 11.4.3.5–2 shows the maximum transverse stress (s11) in the HeE model and the maximum transverse stress for two cases for a simple beam.

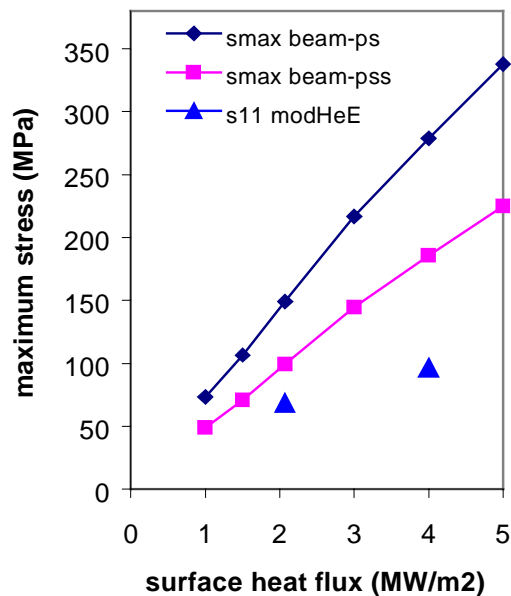


Fig. 11.4.3.5–2 Maximum stress.

Case 1, thermal gradient, no bending, ends constrained (plane strain), and Case 2, thermal gradient, no bending, ends free for axial expansion (plane stress). In this comparison, coolant pressure has been eliminated from the model and there are only thermal stresses.

The plane strain case (top curve) is typical for first walls in which the mass at the back of the channel (away from the heated surface) is thick. This may provide stiffness or material for the fastening scheme to secure the first wall channels to the structure behind it. The main point is, in these cases with a thick back wall, the thin layer at the front of the channel with the thermal gradient is constrained from bending or net axial strain by the larger mass at the back of the channel.

There are several points of discussion and preliminary conclusions regarding these results. Clearly, the primary improvement in reducing the thermal stresses was in permitting bowing of the first wall. The local tailoring had some effect but it was not large. The von Mises stress dropped by only 1% in the 2 MW/m² case and 8% in the 4 MW/m² case. This may be more important

when reductions in the thermal stresses result from further optimization of the configuration or if a more aggressive heat transfer coefficient is used (e.g., $h = 50,000 \text{ W/m}^2\text{-K}$).

The location and magnitude of the maximum stresses indicate that further reductions in the stresses should be possible. For example, the maximum von Mises stress is at the bottom of the coolant passage and results in large part from the pattern of distortion in which the two halves of the channel rotate slightly apart at the top, due to thermal expansion, and together at the bottom. The overall pattern causes local bending strain in the bottom of the coolant passages and the maximum tensile stress occurs at these surfaces. The hard interior corners in the model also contribute.

There are also relatively large axial stresses that result from the overall bending imposed on the mass at relatively uniform temperature at the back of the channel. It is not clear how much this can be reduced. There is probably some hope in reducing these stresses by increasing the width of the central web. Another option is to return to a design with a single coolant passage. A comparative analysis should be done in any case to evaluate the benefit, if any, with respect to thermal stress of the dual passage design.

11.4.3.6 future work — Since the effort in APEX on the refractory alloy design may slow in FY00, the additional work on designing the porous first wall will not be large. Among the tasks to be done are: cases for 12 MPa coolant pressure should be run and the report updated; a round, single passage coolant channel should be evaluated and compared to the dual passage design; and the pressure drop through the Ultramet porous media should be evaluated.

The third point above is an obvious omission in the current report. In the initial work on a design based upon Thermacore's scheme for circumferential flow, the pressure drop was evaluated and found to be satisfactory. That work is not reported here since the design was superceded by the concept with Ultramet's metallized foam and the desire to replace the brazed ball-aggregate with some other porous structure. Some flow data are available for flow of air, a moderate temperature through the Ultramet metallized foam, but this had not yet been evaluated at the time of this report.

11.4.4 swirl tape first wall design. Another method for extended surface heat transfer is to use a swirl tape insert. Swirl tape increases the heat transfer coefficient by increasing the effective flow velocity of the coolant and increasing mixing. There is a large amount of reliable data available on this method. However, the corresponding increase of coolant flow friction factor has to be accounted for [11.4.4-1].

For this calculation, the enhancement in heat transfer coefficient is given by, $h_{en} = 2.18/Y^{0.09}$, and the increase in friction factor is given by $f_{en} = 2.2/Y^{0.406}$, where Y is the twist ratio defined by $Y = \text{pitch}/2 * \text{diameter of the tube}$. Therefore the equivalent $h_{eq} = h_{en} * h$ and equivalent friction factor $f_{eq} = f_{en} * f$, where h and f are heat transfer, and friction factor for simple circular tube, respectively. Y is set at 2 for the thermal hydraulics calculations of the swirl tape first wall design.

Table 11.4.4–1 shows the coolant inlet and outlet temperature at different radial locations of the outboard midplane first wall and blanket zones, where maximum heat flux and wall loading is expected. This table also shows the maximum W-alloy and Li-breeder temperature. With the maximum neutron wall loading of 7.11 MW/m^2 , and maximum surface heat flux of 2.06 MW/m^2 . The swirl-tube first wall coolant velocity range is from 57 to 65 m/s, and the W-alloy maximum temperature is in the range of 1073° to 1242°C . With simple tubes in the blanket, the W-alloy maximum temperature is 1199°C , where the lithium maximum temperature is 1228°C . The W-alloy temperatures at different first wall and blanket locations are within the recommended operating range of $800^\circ\text{C} < T < 1400^\circ\text{C}$.

First wall and blanket system pressure drop as represented by the outboard blanket module was also estimated. Results are shown in Table 11.4.4–2. With the inclusion of pressure drop from turns, contractions, expansions, and frictional losses of first wall, blanket and main helium inlet and outlet pipes the total pressure drop was estimated to be 0.61 MPa which gives a $\Delta P/P$ of 5.1%.

11.4.5 thermal stress analysis of apex first wall design — A thermal stress analysis of a conceptual design for the swirl tape first wall of the APEX blanket was performed using the COSMOS finite element code. The structural model consisted of 2-D beam elements interconnected as shown in Fig. 11.4.5–1 along with the defined temperature distribution provide from heat transfer calculations. The first wall tube has an i.d. of 1.6 cm and an o.d. of 2.2 cm. The beam elements representing the lithium case are $0.2 \times 2.2 \text{ cm}$ for the inner case and $3.8 \times 2.2 \text{ cm}$ for the outer case. The lithium case is supported by a guide structure attached to the VV as shown by the boundary conditions presented in Fig. 11.4.5–1. It is assumed that the guide structure allows free thermal expansion of the lithium case in the vertical and radial directions.

The material selected for the design is tungsten (W5Re) with the following properties at 1000°C :

- Young's modulus = 392 GPa
- Poisson's ratio = 0.267
- Coefficient of thermal expansion = $3.96 \times 10^{-6}/^\circ\text{C}$

The deformed shape and maximum stress due to the assigned temperature distribution and boundary conditions is shown in Fig. 11.4.5–2.

**Table 11.4.4–1 Swirl Tape Outboard First Wall and Blanket Zones Temperatures
(Helium Pressure @ 12 MPa)**

	He-T_{in}	He-T_{out}	W-T_{max}	Li-T_{max}
First wall	800	947	1243	
Module wall			1160	
Blanket zone 1				1158
Tube 1	800	897	1029	
Blanket zone 2				1204
Tube 2	897	974	1076	
Blanket zone 3				1176
Tube 3	974	1002	1078	
Blanket zone 4				1218
Tube 4	1002	1078	1143	
Blanket zone 5				1215
Tube 5	975	1013	1115	
Blanket zone 6				1193
Tube 6	1013	1050	1151	
Blanket zone 7				1190
Tube 7	1013	1073	1174	
Blanket zone 8				1233
Tube 8	1073	1102	1203	
Blanket zone 9				1248
Tube 9	1049	1077	1177	
Blanket zone 10				1237
Tube 10	1077	1100	1199	
Blanket zone 11				1231

Table 11.4.4–2 Swirl Tape First Wall and Blanket Pressure Drop Estimate, Represented by the Outboard Blanket Configuration (Helium Pressure @ 12 Mpa)

	MPa
First wall	0.029
Blanket tubes	0.212
Plenum	0.0066
14 turns, 6 contractions and 6 expansion (@ V-He=60 m/s)	0.25
Total piping 40 m long (@ V-He=40 m/s)	0.11
Total ΔP	0.61
$\Delta P/P$	0.05
Total pumping power, MW	286.5
Pumping power/thermal power	0.078

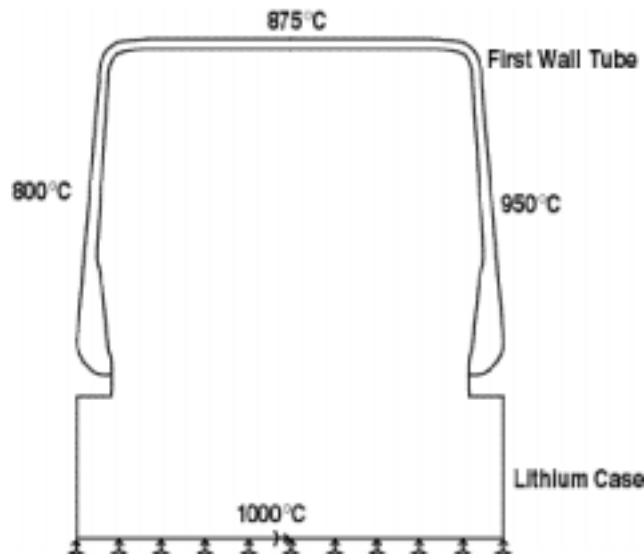


Fig. 11.4.5–1 Structural model of APEX blanket concept for the outboard blanket module.

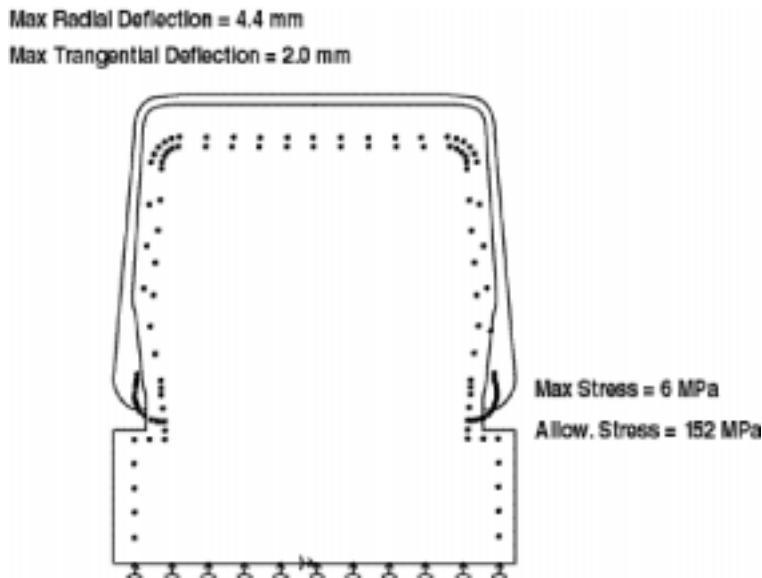


Fig. 11.4.5–2 Deformed shape and max. thermal stress in APEX blanket concept, represented by the outboard blanket module.

The tangential thermal growth of the first wall tube of 2.0 mm requires that the blanket modules be installed with 4.0 mm gaps in the cold condition to prevent contact with one another during operation. The radial thermal growth of the plasma facing tube is 4.4 mm.

Since the proposed support structure will allow free thermal expansion of the lithium case, only the temperature difference between the first wall tube and lithium case will induce thermal stresses. The maximum thermal stress occurs in the outboard first wall tube at its junction to the lithium case and is on 6 MPa. This result is consistent to the approach taken in Section 11.4.3.

With the understanding that W-alloy would be considered as brittle material after a low fluence of irradiation, it has been proposed that the stress criteria for evaluating calculated stress intensities for tungsten materials be taken to be one-half the ultimate stress at temperature for welded joints and two-thirds the ultimate stress away from joints. Adopting these criteria, the allowable stress at the weld joint due to all load combinations is 150 MPa at 1000°C.

Although the proposed concept for supporting the blanket induces low thermal stress, details of how to implement the support concept will certainly result in higher thermal stresses. Also, the stresses due to dead weight, pressure, and disruption loads have yet to be calculated. This will be performed in the next phase of the design.

11.5 Nuclear Analysis

In performing the helium-cooled refractory alloy first wall and blanket design, the design was by iteration between the areas of mechanical design, thermal-hydraulics, and nuclear analysis. This section presents the results of nuclear analysis. The basic nuclear performance parameters of tritium breeding ratio (TBR), nuclear heating and radiation damage are presented.

11.5.1 introduction — In this section, we assess the impact of using various refractory metals on the nuclear heating profiles across the blanket and power multiplication (PM) and on the tritium breeding profiles and TBR. The refractory metals considered with liquid lithium breeder are W, TZM, and Nb-1Zr. The impact of Li-6 enrichment on these profiles and on TBR and PM is also assessed. Comparison of these nuclear characteristics is also made to other liquid breeders (Flibe and Li-Sn). In addition, we assess the damage indices, expressed in terms of DPA, helium, and hydrogen production rates at several locations including the vacuum vessel (VV) and TF coil case with various refractory metals and breeders; and comparison is made to the liquid first wall and blanket concept.

11.5.2 calculation model — The 1-D calculation model used in the outboard blanket analysis is shown in Fig. 11.5.2–1. Liquid lithium with tungsten structure and helium coolant are used as the

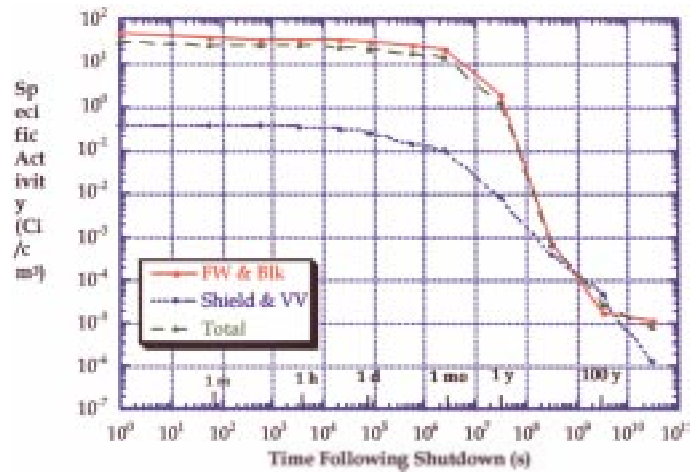


Fig. 11.5.2–1 The outboard radial build of the He-cooled refractory alloy first wall and blanket concept (1-D cylindrical model).

reference case. The volume fraction of materials in each outboard zone is given in Table 11.5.2–1. The variation of volume fraction resulted from variation in size of tubing for the liquid breeder and the helium coolant at various locations. The first wall facing the plasma is 2.2-cm thick and is cooled with helium followed by a solid wall (module wall) of 0.2-cm thick. The blanket zones vary in thickness as 1.5 cm, 1.8 cm, and 3.7 cm while the tube zones are 1.3-cm thick, as shown in Fig. 11.5.2–1. The total blanket thickness is ~57 cm, followed by the transitional zone (23-cm thick), the plenum zone (40-cm thick), and the shield (10-cm thick). In all cases, the VV is made of 2-cm thick outer walls with an internal 26-cm thick zone consists of 60:40 316SS:Water. The TF coil case is made of SS316LN and epoxy is used as the insulator.

Table 11.5.2–1 Volume Fraction of Materials in Various Outboard Zones

Zone Name	Structure	Breeder	Coolant (Helium)
First wall	0.167	—	0.831
Module wall	1.0	—	—
Blanket Zone 1	0.013	0.975	0.04
Tube Zone 1, 2, 3, 4	0.32	0.215	0.465
Blanket Zone 2	0.022	0.924	0.054
Blanket Zone 3	0.031	0.902	0.067
Blanket Zone 4	0.04	0.879	0.081
Blanket Zone 5	0.05	0.856	0.094
Transitional zone	0.7	—	0.3
Plenum zone	0.4	—	0.6
Shield zone	0.8	—	0.2

11.5.3 tritium breeding and effect of structural material — The best outboard local TBR performance is with W and Li breeder. The TBR increases with Li-6 enrichment and start to saturate at a value of ~1.43 when Li-6 enrichment is ~35%. It reaches an optimal value of ~1.45 at ~50% Li-6 enrichment. Neutrons slowed down by the W structure are absorbed mainly by Li-6 via Li-6 (n, α) reactions. Even at natural Li-6 enrichment (TBR < 1), most of the contribution to TBR is from Li-6 (T6), as can be seen from Fig. 11.5.3–1. This is also apparent from Fig. 11.5.3–2 which shows the tritium production profiles across the breeding zone for the case with 35% Li-6 enrichment.

Using TZM and Nb-1Zr results in ~4% and ~15% decrease in TBR, respectively, as shown in Fig. 11.5.3–3 (35% Li-6, TZM: TBR ~1.37; Nb-1Zr: TBR ~1.21). Note from this figure that, while the contribution from Li-7 to the local TBR (T7) is ~0.2 among various structural materials, the reduction in TBR is mainly due to reduction in TBR from Li-6 (T6). T6 is the largest in the W case while T7 is relatively the largest in the TZM case. This is also apparent from the T6 and T7 profiles across the blanket depicted in Figs. 11.5.3–4 and 11.5.3–5, respectively.

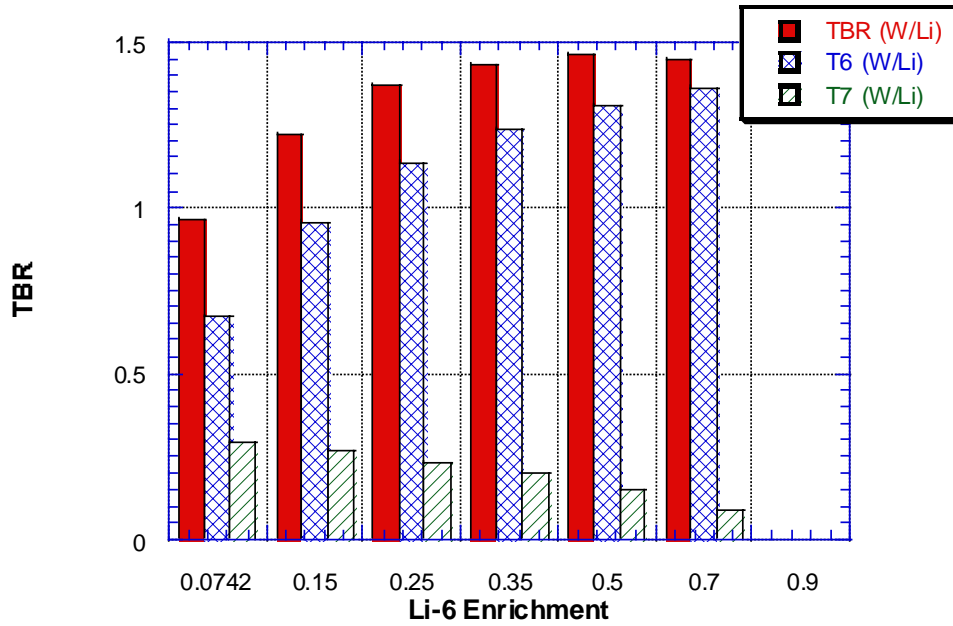


Fig. 11.5.3-1 Outboard local TBR with W/Li structure/breeder as a function of Li-6 enrichment.

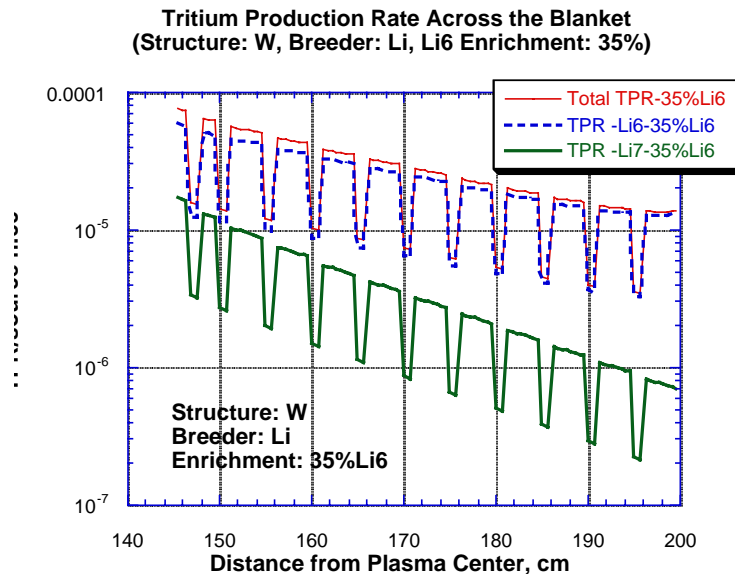


Fig. 11.5.3-2 Profiles of outboard tritium production rate across the blanket region and contribution from T6 and T7 (W structure- 35% Li-6).

**Total Tritium Breeding Ratio and Contribution from Li6 and Li7
For Various Refractory Structural Materials**

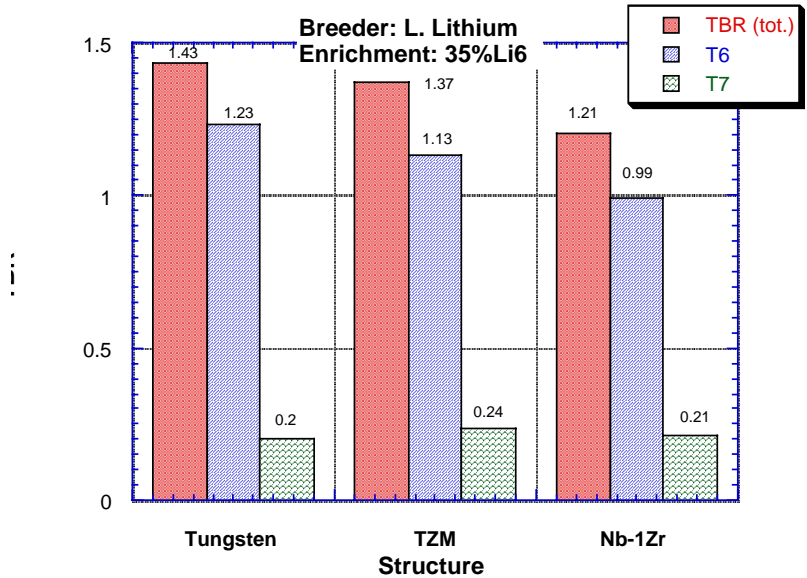


Fig. 11.5.3–3 Outboard local TBR and contribution from Li-6 (T6) and Li-7 (T7) for various refractory metals structure.

**Tritium Production Rate from Li-6 Across the Blanket
For Various Structural Materials
(Enrichment: 35% Li6, Breeder: L. Lithium)**

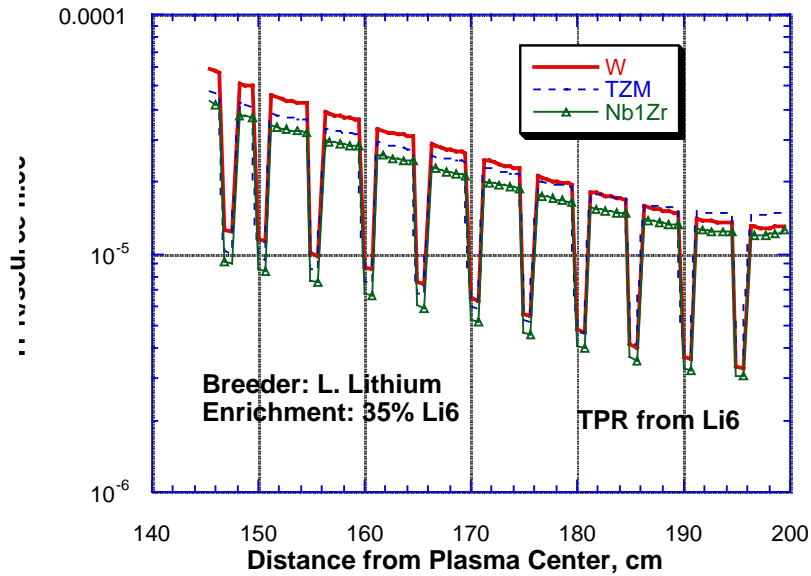


Fig. 11.5.3–4 Profiles of outboard tritium production rate from Li-6 (T6) for various structural materials.

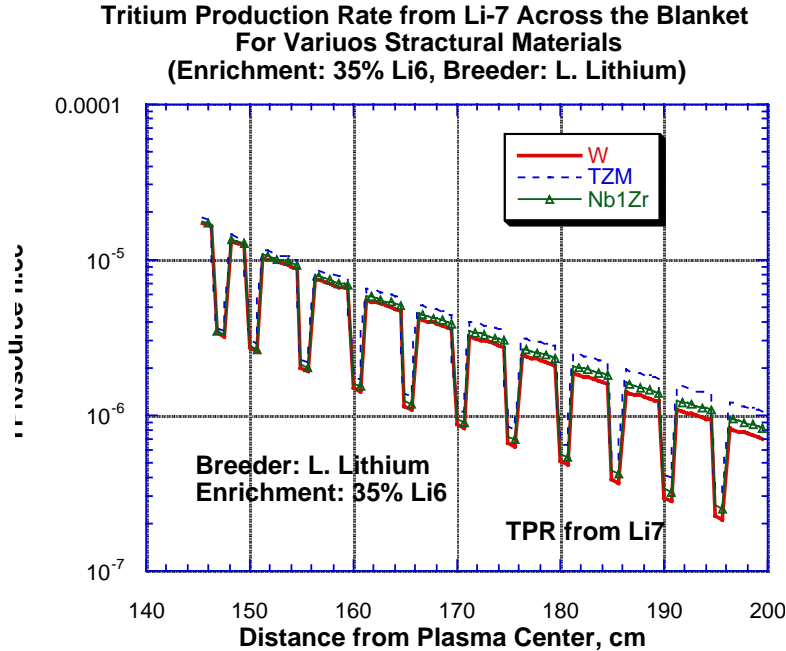


Fig. 11.5.3–5 Profiles of the outboard tritium production rate from Li-7 (T7) for various structural materials.

11.5.4 nuclear heating and effect of structural materials — For an average wall load of 10 MW/m^2 , nuclear heating profiles and PM of the outboard blanket have been calculated throughout the various zones shown in Fig. 11.5.2–1. Smearred nuclear heating rate is defined as the average power deposition rate at a particular location in a given zone when the materials given in Table 11.5.2–1 are homogenized in the calculation for that zone. Heterogeneous rates, Ht_j , for a particular material j , are those when the volume fraction of that material, F_j is taken into consideration ($Ht_j = \text{Homogeneous value, } Ho_j/F_j$).

In the W/Li system, the largest smearred heating rate occurs at the front module wall and is $\sim 90 \text{ W/cc}$ for an average wall load of 10 MW/m^2 , as can be seen from Fig. 11.5.4–1. Neutron heating dominates the total heating rate in the blanket zones due to absorption in the Li-6. Gamma heating is the dominant contributor in the first wall, module wall, rod zones, transitional zone, plenum, and the shield.

In the blanket zones, W structure gives the highest heat deposition rates. The values in the TZM case are lower but comparable to the W case. It tends to be the largest toward the back blanket zones, the transitional, plenum, and the shield zones. These features are shown in Fig. 11.5.4–2. As shown in Fig. 11.5.4–3, the heating rates in the tube zones (32% structure, 47% He, 21% Li) when either TZM or Nb-1Zr is used as structure are comparable but are a factor of 1.5 lower compared to the W case (more gammas in this case). The maximum heating rates in the TZM (or Nb-1Zr) structure is $\sim 40 \text{ W/cc}$, which is a factor of 2.2 lower than in the W case.

**Total Nuclear Heating rate Across the Blanket/Shield System
(Structure: W)**

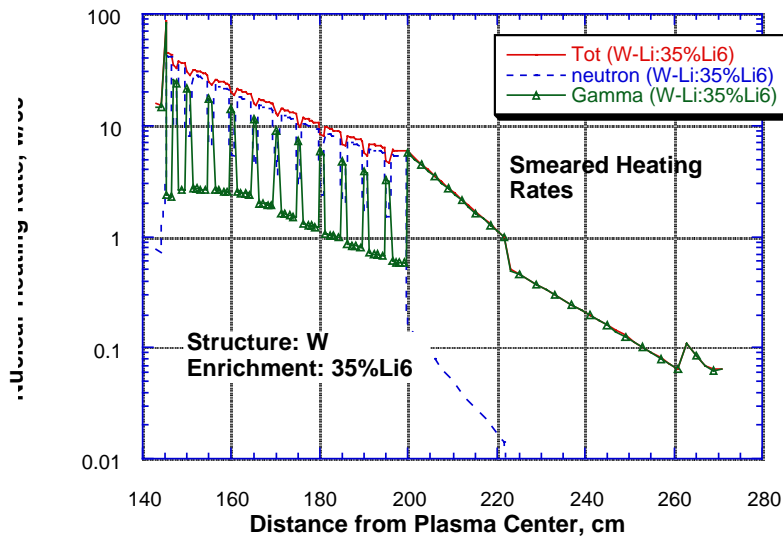


Fig. 11.5.4–1 Total nuclear heating rate profiles across the outboard blanket, transitional zone, plenum, and shield system (W/Li:structure/breeder).

**Total Nuclear Heating rate Across the Blanket/Shield System
With various Structural Materials**

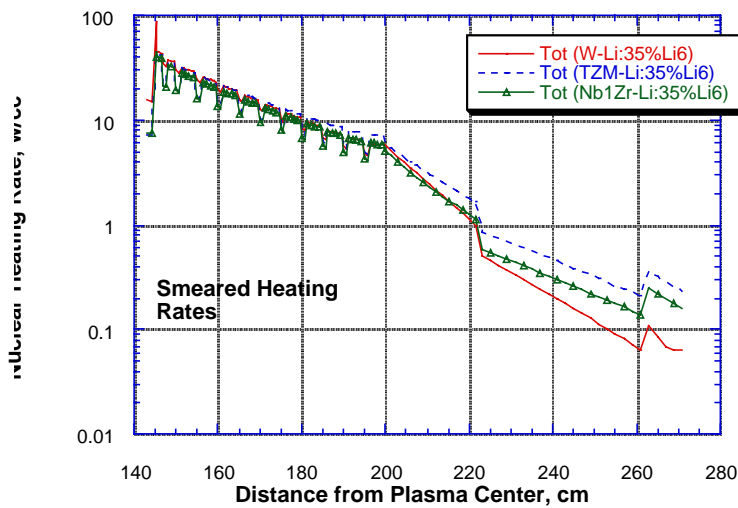


Fig. 11.5.4–2 Profiles of the total nuclear heating rates across the outboard blanket, transitional zone, plenum, and shield for various structural materials.

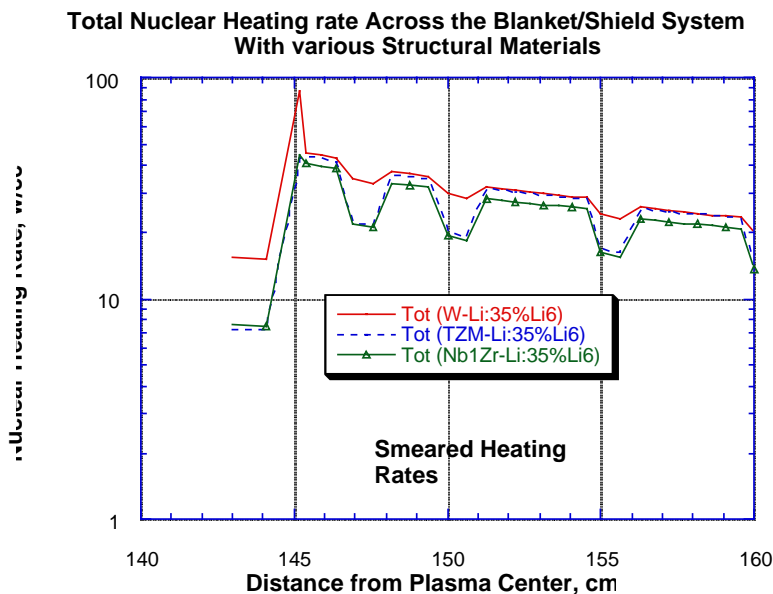


Fig. 11.5.4-3 Profiles of the total nuclear heating rates across the outboard first wall and front part of the blanket for various structural materials.

When outboard volume fractions of the breeder and structure are considered, approximate heterogeneous heating rates can be derived from the smeared heating rates in a particular zone as discussed earlier. According to Figs. 11.5.4-4 and 11.5.4-5, the maximum heating rate in the W structure is ~90 W/cc and is ~50 W/cc in the breeder zones. Neutron heating is dominant in the breeder while gamma heating is dominant in the tungsten structure

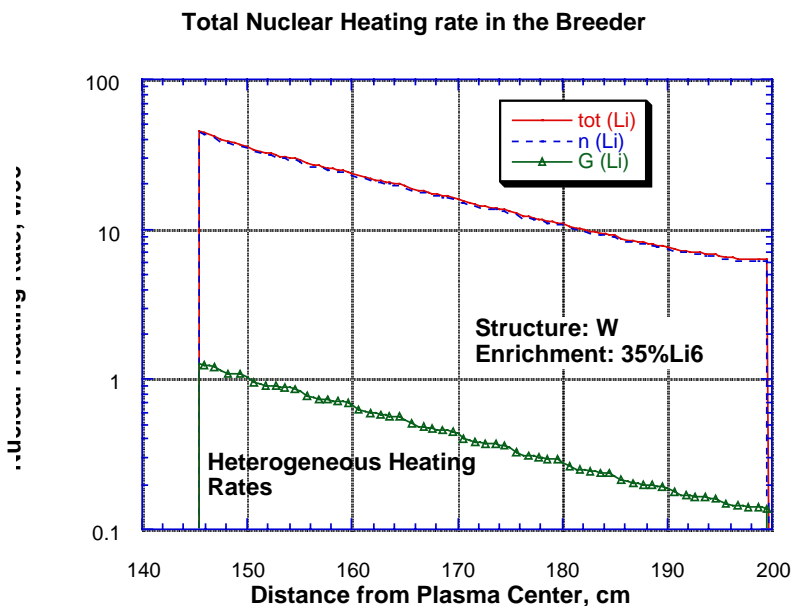


Fig. 11.5.4-4 Profiles of the total heterogeneous nuclear heating rates in the outboard breeder and contribution from neutrons and gamma heating (W/Li system, 35% Li-6 enrichment).

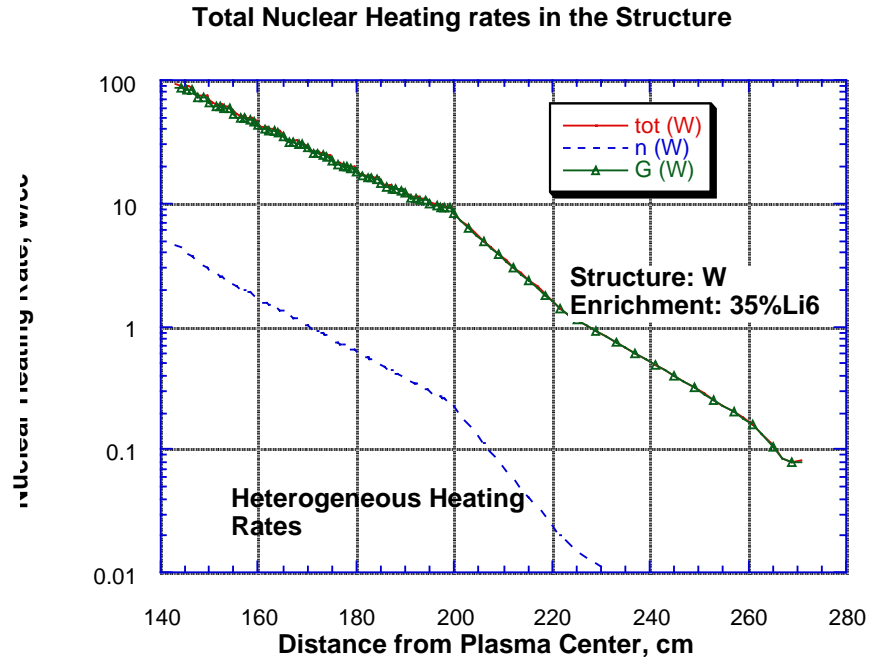


Fig. 11.5.4-5 Profiles of the total heterogeneous nuclear heating rates in the outboard tungsten structure and contribution from neutrons and gamma heating (W/Li system, 35% Li-6 enrichment).

11.5.5 effect of breeders on tritium breeding and nuclear heating — Two other liquid breeders are considered, in addition to liquid lithium. They are the Flibe and Li-Sn and tungsten structure is used as the refractory metal. Figure 11.5.5-1 shows the TBR and PM as a function of the Li-6 enrichment. The TBR is low (0.25) for Sn-Li with natural Li-6 but it increases rapidly with increasing Li-6 enrichment and reaches a value of ~1.15 at 90% Li-6 enrichment. Clearly the “local” outboard TBR value obtained from 1-D calculations is still marginal and tritium self-sufficiency cannot be granted if penetrations and coverage fraction of the blanket is taken into consideration. In Flibe case, the situation is improved where TBR shows a steady increase with Li-6 enrichment (~0.45 at natural Li-6 and ~1.21 at 90 % Li-6). The same concern still holds for the Flibe, *i.e.*, breeding appears to be marginal. The Li breeder shows the largest TBR. The TBR in this case saturates around 35% Li-6 (TBR ~ 1.43) and then starts to decrease with Li-6 enrichment (see Table 11.5.5-1). Note that in contrast to the GMD thick liquid first wall and blanket concept in which large amount of liquid is facing the plasma, the TBR in Li and Flibe increases with Li-6 enrichment due to the presence of the solid first wall in the He-Cooled first wall and blanket concept. This layer tends to slow down high-energy neutrons via inelastic scattering and they end up being absorbed in Li-6 via Li-6 (n,α) reactions. In the thick liquid concept, however, large amount of Li-7 (*i.e.*, smaller Li-6 enrichment) improves the neutron economy via Li-7 (n,n'α)t reaction which occurs at high energy and there TBR is the largest at natural Li-6 enrichment.

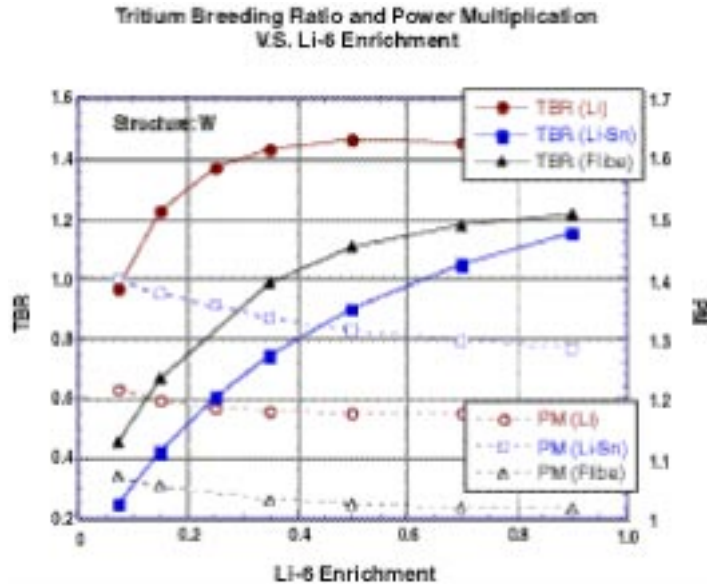


Fig. 11.5.5-1 The 1-D outboard TBR and PM as a function of Li-6 enrichment for several breeders.

Table 11.5.5-1 1-D Outboard TBR and PM in the He-Cooled Refractory Metal First Wall and Blanket Concept

	Natural Li-6			35% Li-6			90% Li-6		
	Li	Flibe	Sn-Li	Li	Flibe	Sn-Li	Li	Flibe	Sn-Li
TBR	0.96	0.45	0.25	1.43	0.99	0.74	1.42	1.21	1.15
PM	1.22	1.07	1.40	1.18	1.03	1.33	1.16	1.02	1.30

The contribution to the total local TBR is dominated by tritium breeding from Li-6 (T6) even at natural Li-6 enrichment. This can be seen from Fig. 11.5.5-2 which shows the contribution to TBR from Li-6 (T6) and Li-7 (T7) for the three breeders.

The PM is the largest in the Li-Sn case (PM ~1.4 at natural Li-6 enrichment). This is advantageous from the viewpoint of improving the thermal cycle and its efficiency but the Li-Sn breeder, even at 90% Li-6, has a marginal TBR. Generally, the PM decreases slightly with Li-6 enrichment. At natural Li-6 enrichment, PM is ~1.22 (Li), ~1.40 (Li-Sn) and ~1.07 (Flibe). At 90% Li-6 enrichment, PM is ~1.16 (Li), ~1.3 (Li-Sn) and ~1.02 (Flibe), *i.e.*, power deposited in the blanket/shield system when Li-Sn is used as a breeder is larger by ~15% and by ~31% than Li and Flibe case, respectively, with natural Li is used and is larger by ~12% and by ~27% than Li and Flibe case, when Li-6 is enriched to 90%. Note in particular that the PM is the lowest in the Flibe case (~1.02) which indicates that the incident neutron power to the system has only increased by 2%.

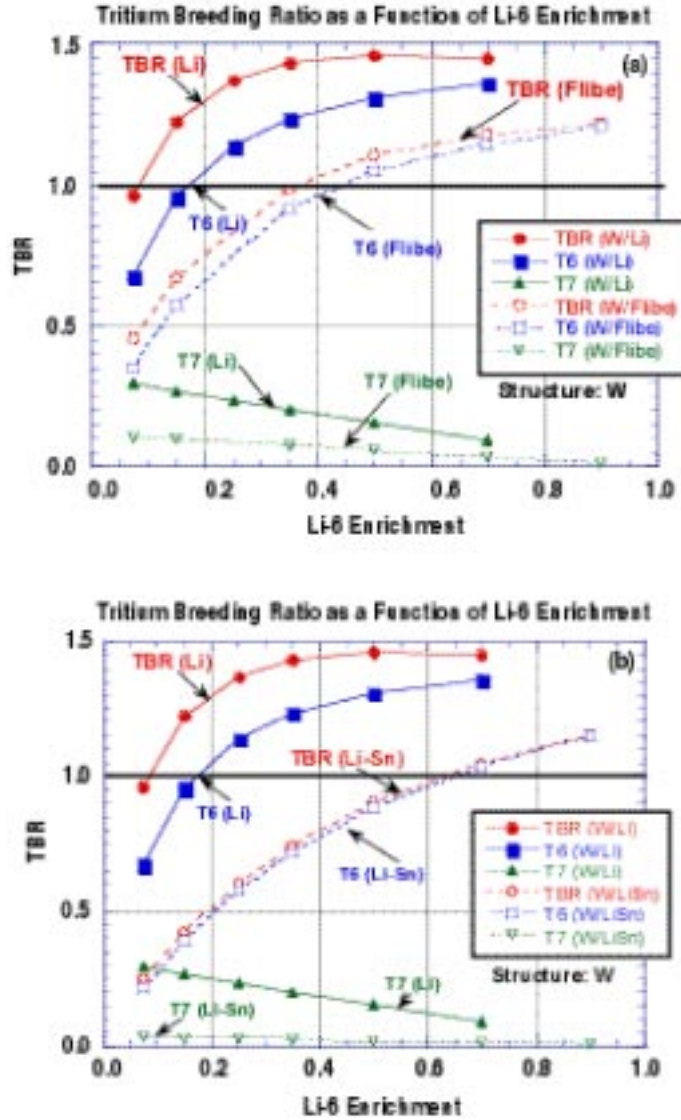


Fig. 11.5.5–2 The 1-D outboard TBR as a function of Li-6 enrichment and contribution from Li-6 (T6) and Li-7 (T7): (a) Li and Flibe, (b) Li and Li-Sn.

The large PM in the Li-Sn breeder case is due to the large $\text{Sn}(n,\gamma)$ reaction rate, which generates larger gamma-ray flux. The gamma heating is the main contributor to the total heating in the first wall and blanket/shield system as can be seen from Fig. 11.5.5–3. This figure shows the total power deposited in the system per unit height (w/cm) in the poloidal direction as a function of the Li-6 enrichment and for neutron wall load of 10 MW/m^2 . Here a comparison is made between Li and Sn-Li. Still Li-Sn gives larger power deposition rate than Li (by a factor of 1.15 at 35% Li-6 enrichment). In addition, the contribution from gamma heating in the Li-Sn case is always larger than the contribution from neutron heating, but decreases with Li-6 enrichment. At 90% Li-6 enrichment, the contributions from gamma heating and neutron heating are comparable. As for Li case, the contribution from neutron heating is dominant above $\sim 10\%$ Li-6 enrichment.

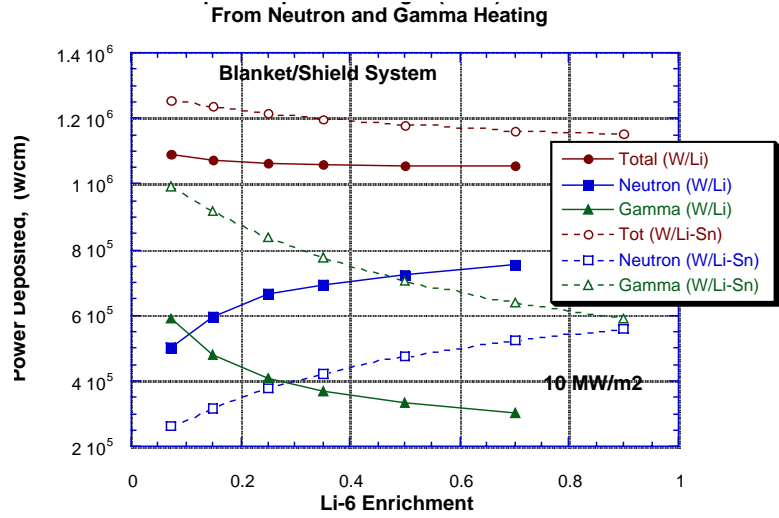


Fig. 11.5.5-3 Total power deposited in the outboard first wall and blanket/shield system per unit height as a function of the Li-6 enrichment.

As for the power deposited in the breeder only, it increases with Li-6 enrichment, as shown in Fig. 11.5.5-4. It is larger in the Li-Sn breeder than in the Li breeder. This power is due mainly to neutron interaction in the case of Li (very small contribution from gamma interaction) while contribution from neutrons and gamma heating is comparable in the Li-Sn breeder. Note in particular that the gamma heating in the Li-Sn breeder is dominant when Li-6 enrichment is below 25%.

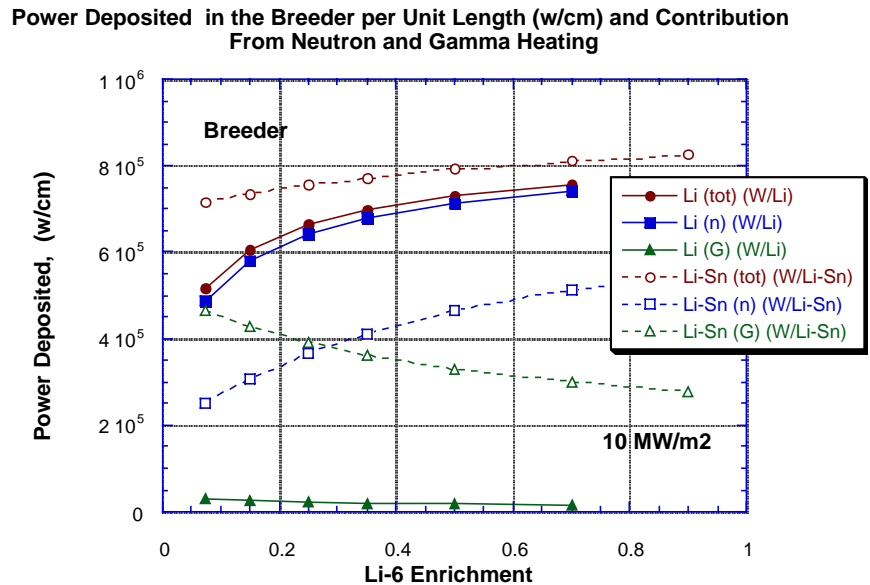


Fig. 11.5.5-4 Total power deposited in the outboard breeder per unit height as a function of the Li-6 enrichment.

Total Power deposited in the outboard structure (W) decreases with Li-6 enrichment. This can be seen from Fig. 11.5.5–5. It is due mainly to gamma heating, which is enhanced in the Li-Sn case. Gamma production rate via $\text{Sn}(n,\gamma)$ is noticeably large and slightly decreases with Li-6 enrichment [$\text{Li-6}(n,\alpha)$ and $\text{Sn}(n,\gamma)$ are competing reactions]. The large amount of gamma production in Sn tends to increase total PM through large contribution from gamma heating in the breeder and the W structure with very little contribution from neutrons heating.

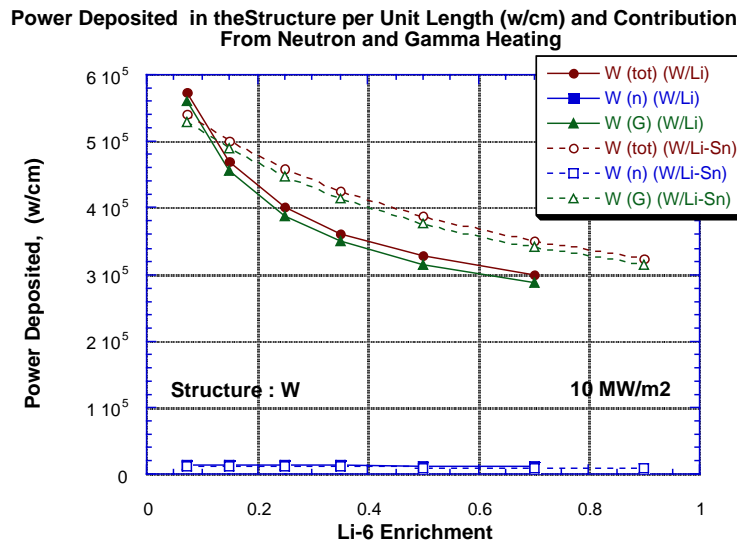


Fig. 11.5.5–5 Power deposited in the outboard tungsten structure per unit height and contribution from neutrons and gamma heating.

11.5.5.1 damage parameters and effect of structural materials — The impact of using various refractory metal as structure on the damage parameters at various locations [First Wall, Module Wall, VV, superconducting magnet (SCM) Case] has been assessed. The parameters considered are the DPA, helium, and hydrogen production rates. The reference case is with tungsten structure and liquid lithium (35% Li-6 enrichment) as the breeder with helium cooling. In addition, the impact of using other breeders on these parameters was also assessed. These breeders are Flibe (90% Li-6 enrichment) and Li-Sn (90% Li-6 enrichment). A comparison of these parameters to the GMD thick liquid first wall and blanket concept was also made. At 10 MW/m^2 wall load, the DPA rate at the first wall is: W 56.3 DPA/FPY, TZM 89.0 DPA/FPY, and Nb-1Zr 55.5 DPA/FPY. Tungsten shows the lowest DPA rate across the blanket/shield system. The TZM shows the highest damage rate while Nb-1Zr has a low rate at the first wall but DPA rate resumes the TZM values at deeper locations, as can be seen from Fig. 11.5.5.1–1, which depicts the DPA profiles across the blanket, transitional zone, plenum, and the shield. The DPA cross sections for the three structural materials considered are shown in Fig. 11.5.5.1–2.

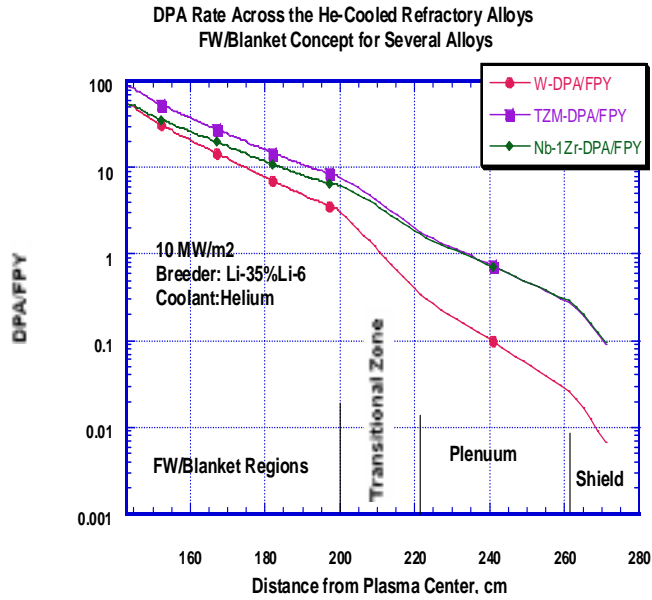


Fig. 11.5.5.1–1 The DPA profiles across the outboard blanket, transitional zone, plenum, and the shield for various structural materials.

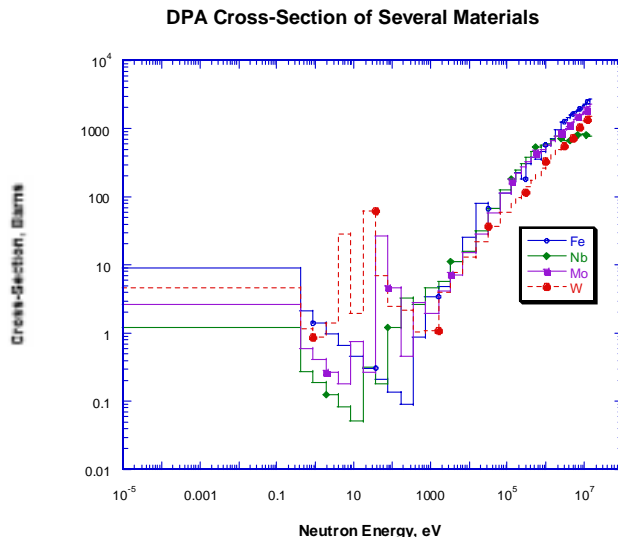


Fig. 11.5.5.1–2 The DPA cross section of several structural materials.

At 10 MW/m^2 the helium production rate at the first wall is: W 21.8 appm/FPY, TZM 384.1 appm/FPY, and Nb-1Zr 372.8 appm/FPY. The tungsten shows the lowest helium production rate. At the first wall, its value is more than an order of magnitude less than TZM and Nb-1Zr cases (~ 2 orders of magnitude at back locations, see Fig. 11.5.5.1–3). The helium production rates in TZM and Nb-1Zr are similar due to the similarity in their cross sections as can be seen from Fig. 11.5.5.1–4.

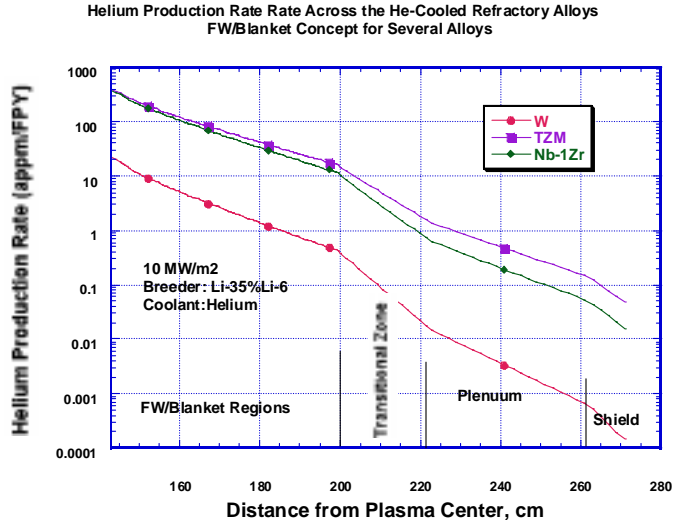


Fig. 11.5.5.1–3 The helium production profiles across the outboard blanket, transitional zone, plenum, and the shield for various structural materials.

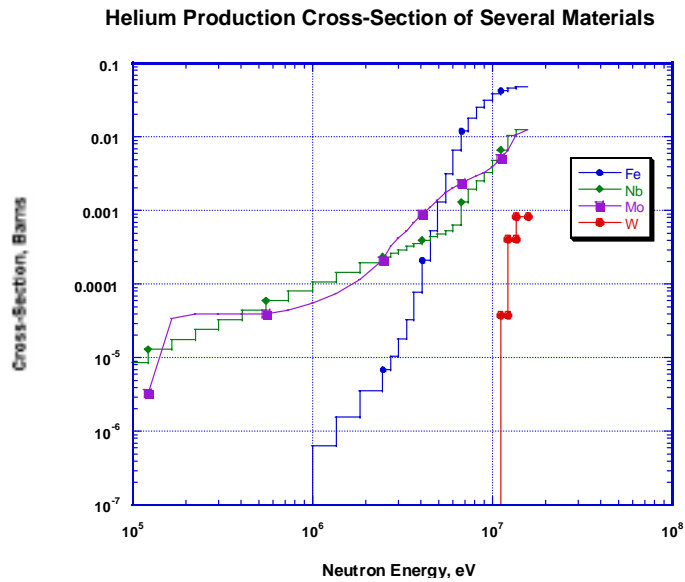


Fig. 11.5.5.1–4 The helium production cross section of several structural materials.

At 10 MW/m^2 the hydrogen production rate at the first wall is: W 78.4 appm/FPY, TZM 3008.9 appm/FPY, and Nb-1Zr 2052.7 appm/FPY (see Fig. 11.5.5.1–5). The tungsten shows the lowest hydrogen production rate. At the first wall, its value is more than an order of magnitude less than TZM and Nb-1Zr cases (~ 2 orders of magnitude at back locations, see Fig. 11.5.5.1–6). The hydrogen production rate in Nb-1Zr is lower than in TZM by a factor of 1.5 at the first wall (~ 7 at back locations).

Hydrogen Production Rate Rate Across the He-Cooled Refractory Alloys
FW/Blanket Concept for Several Alloys

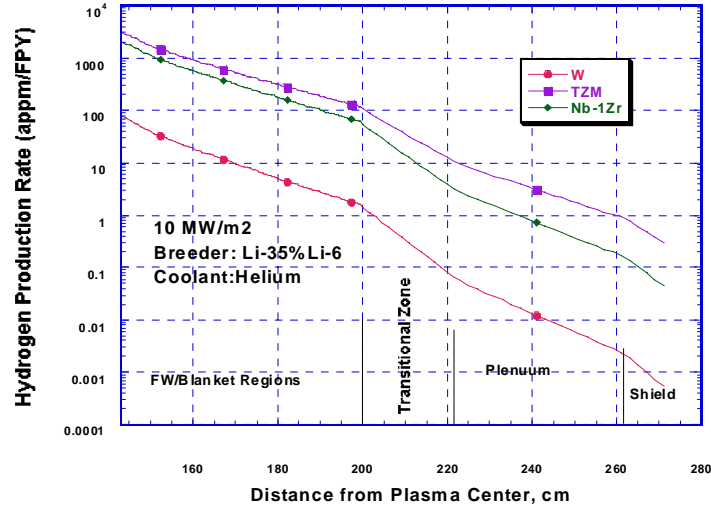


Fig. 11.5.5.1–5 The hydrogen production profiles across the outboard blanket, transitional zone, plenum, and the shield for various structural materials.

Hydrogen Production Cross-Section of Several Materials

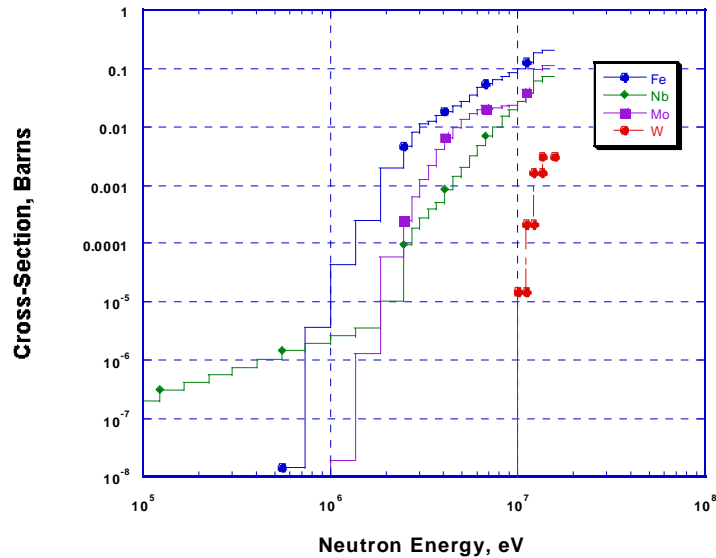


Fig. 11.5.5.1–6 The hydrogen production cross section of several structural materials.

The damage parameters at the VV wall, the casing of the SCM “TF coil,” and the Cu stabilizer were also calculated for several structural materials and the results are shown in Table 11.5.5–2. Also shown in the table are the corresponding damage parameters in the GMD thick liquid First wall and blanket concept in which 42-cm thick liquid Flibe first wall and blanket is placed in front of the backing solid wall and shield and ferritic steel is used as the

Table 11.5.5–2 Damage Parameters in the Helium-Cooled Refractory Metal First Wall and Blanket Concept with Various Structural Material and Comparison to the Thick Liquid First Wall and Blanket Concept for the Outboard Blanket

Displacement per Atom (DPA/FPY) – 10 MW/m²					
Location	He-Cooled Refractory Alloys First wall and blanket Concept (Li- Breeder- 35% Li-6)			Thick Liquid Wall Concept Flibe (Natural Li-6)	
	W	TZM	Nb-1Zr	Location	Ferritic Steel
First wall	56.3	89.1	55.5		
Module wall	50.3	81.8	51.6	Solid wall	3.6 /142
VV case	0.009	0.07	0.06	VV case	0.01/0.26
SCM case	0.00007	0.0008	0.0004	SCM case	0.0001/0.003
Cu-stabilizer	0.000001	0.00001	0.000005	Cu-stabilizer	0.00001/0.001
Helium Production Rate (appm/FPY) – 10 MW/m²					
Location	He-Cooled Refractory Alloys First wall and blanket Concept (Li- Breeder- 35% Li-6)			Thick Liquid Wall Concept Flibe (Natural Li-6)	
	W	TZM	Nb-1Zr	Location	Ferritic Steel
First wall	21.8	384.1	372.8		
Module wall	18.5	341.8	324	Solid wall	20.8/1564 ^(a)
VV case	0.096	0.64	0.43	VV case	0.02/0.645
SCM case	0.0005	0.005	0.003	SCM case	0.0002/0.008
Hydrogen Production Rate (appm/FPY) – 10 MW/m²					
Location	He-Cooled Refractory Alloys First wall and blanket Concept (Li- Breeder- 35% Li-6)			Thick Liquid Wall Concept Flibe (Natural Li-6)	
	W	TZM	Nb-1Zr	Location	Ferritic Steel
First wall	78.4	3009	2053		
Module wall	66.6	2671	1782	Solid Wall	85/6882
VV case	0.09	0.89	0.30	VV Case	0.07/2.7
SCM case	0.001	0.01	0.004	SCM Case	0.0009/0.03

^(a)With/without liquid layer.

structural material. The parameters in this concept for a bare backing wall (no thick liquid first wall and blanket) are also shown for comparison.

In the helium-cooled refractory alloy first wall and blanket concept, the DPA at the outboard first wall with tungsten structure is a factor of 1.6 lower than the TZM and Nb-1Zr cases. It is a factor of ~7 lower at the VV. With tungsten, the helium production rate at the first wall is a factor of ~18 lower than the TZM and Nb-1Zr cases. It is a factor of ~6 and ~4 lower at the VV than the TZM and Nb-1Zr cases, respectively (TZM values are ~40% larger than the Nb-1Zr case). As for the hydrogen production rate, the value at the first wall with tungsten structure is a factor of ~38 and ~26 lower than the TZM and Nb-1Zr cases, respectively. It is a factor of ~10 and ~3 lower at the VV than the TZM and Nb-1Zr cases, respectively. Generally, the damage parameters are larger with the TZM structure than the Nb-1Zr.

The DPA rate, helium and hydrogen production rates at the first wall with the tungsten structure are 56 DPA/FPY, 22 appm/FPY, and 78 appm/FPY, respectively. The corresponding values in the thick first wall and blanket concept at the backing first wall are 3.6 DPA/FPY, 21 appm/FPY, and 85 appm/FPY, respectively. Thus the DPA rate at the first wall is a factor of ~16 larger in the helium-cooled concept as compared to the thick liquid first wall and blanket concept. However, the helium and hydrogen production rates are comparable in the two concepts. Also, these damage parameters are comparable at the VV and the magnet casing.

Without the liquid layer in the liquid first wall and blanket concept, the damage parameters in the backing solid wall (ferritic steel) are 142 DPA/FPY, 1564 appm/FPY, and 6882 appm/FPY, respectively, *i.e.*, they are larger than the protected walls (*i.e.*, with the liquid layer) by a factor of 40, 74, and 80, respectively. This shows the effectiveness of attenuating the damage parameters in the presence of the liquid walls by ~1–2 orders of magnitudes.

11.5.7 damage parameters and effect of type of breeder — The damage parameters at various locations were estimated in the reference blanket (tungsten structure, liquid lithium breeder with 35% Li-6 enrichment) but with two other breeders, namely, Flibe (90% Li-6 enrichment) and Li-Sn (90% Li-6 enrichment). The results are shown in Figs. 11.5.7–1 through 11.5.7–3 for the DPA, helium, and hydrogen production rates, respectively.

The figures show that the damage parameters at the first wall and Module Wall are similar among the three breeders. This is expected since the breeders are present behind these walls and the reflected components of the neutron flux to these walls from the breeding zones are similar. However, the damage parameters at the VV and TF Coil are higher with the lithium breeder than with the Flibe breeder by a factor of 6–10. On the other hand, the damage parameters at the VV and TF coil are larger with the Li-Sn breeder than with the Flibe breeder by a factor of 1.3–2.7. This shows that the liquid lithium is the less effective material in attenuating the nuclear field at the VV and TF coil relative to the other breeders while the Flibe is the most effective material in reducing the damage at these locations.

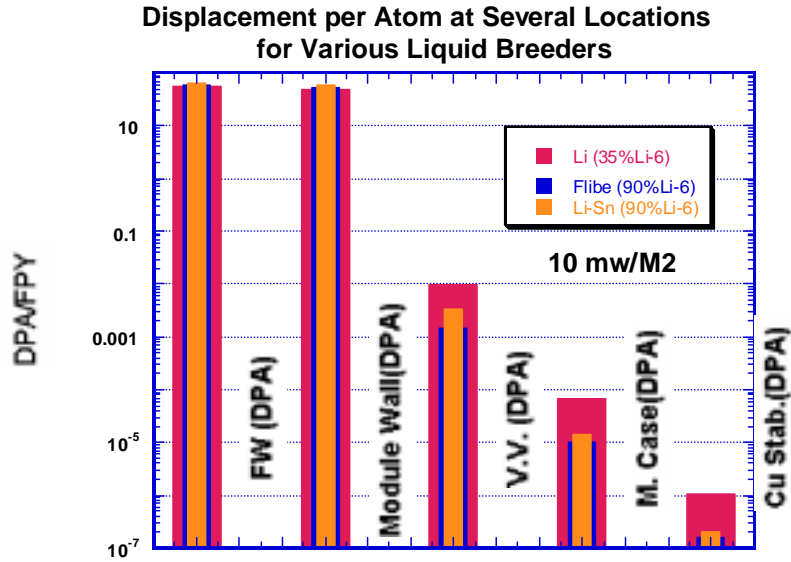


Fig. 11.5.7-1 The DPA rate at various locations with several breeders in the helium-cooled refractory metal first wall and blanket concept at the outboard.

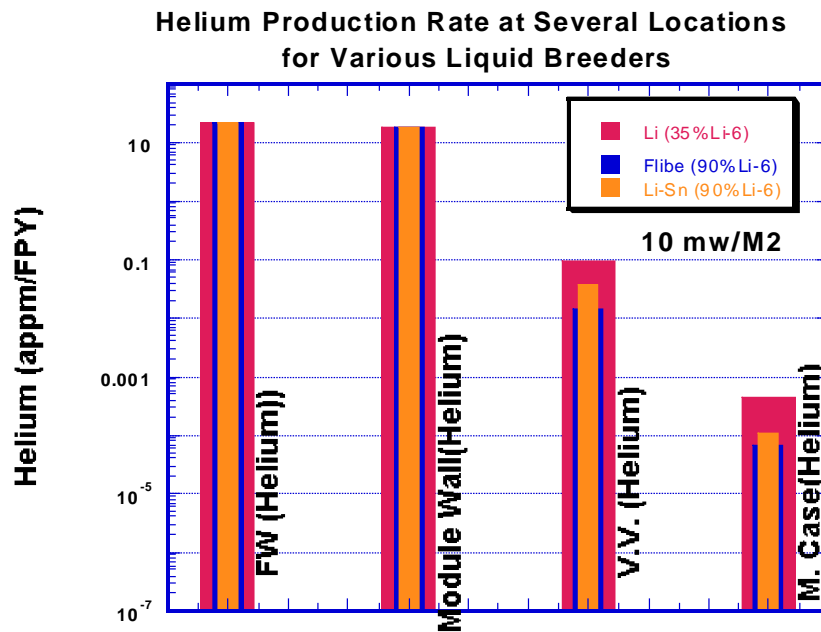


Fig. 11.5.7-2 The helium production rate at various locations with several breeders in the helium-cooled refractory metal first wall and blanket concept at the outboard.

Hydrogen Production Rate at Several Locations for Various Liquid Breeders

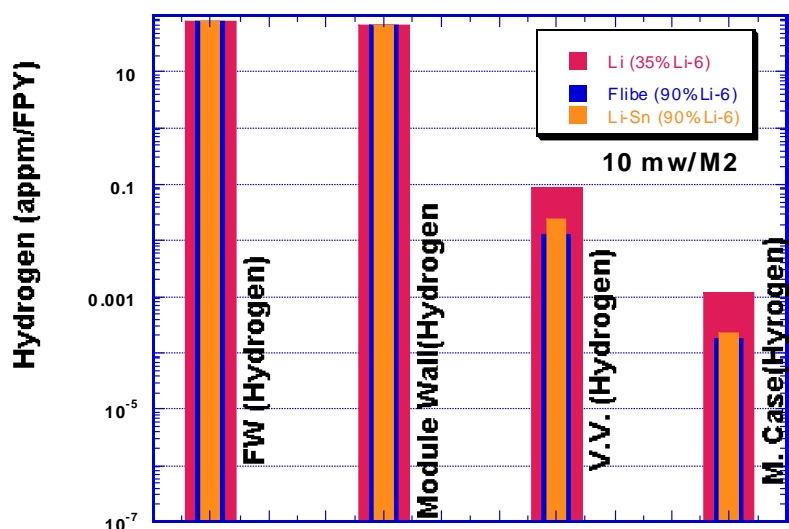


Fig. 11.5.7-3 The hydrogen production rate at various locations with several breeders in the helium-cooled refractory metal first wall and blanket concept at the outboard

11.6 Activation Analysis

11.6.1 introduction — Activation analysis was performed for the He-cooled refractory alloy concept. The calculations used cylindrical geometry. Calculations were performed assuming a neutron wall loading of 10 MW/m^2 at the first wall. The analysis used the W-5Re alloy as the structure material. The elemental composition of the W-5Re alloy is shown in Table 11.6.1-1. The first wall damage for W-alloy, as shown in Fig. 11.5.5.1-1, is at about 60 dpa/FPY normalized to the neutron wall loading of 10 MW/m^2 . Therefore, at a radiation damage limit of 200 dpa, the W-alloy first wall and blanket can be projected to have a lifetime of 3.3 FPY. On the other hand, the shield and VV are assumed to stay in place for 30 FPY. For the following calculations, the induced radioactivity of the fusion power core component was evaluated at a lifetime of 5 FPY. Shorter lifetime will have proportionally lower induced radioactivity. The radial build of the 1-D model used in the calculation is shown in Fig. 11.5.2-1. Neutron transport calculations were performed using the discrete ordinates neutron transport code ONEDANT. The analysis uses a P_3 approximation for the scattering cross sections and S_8 angular quadrature set.

The neutron flux obtained from the neutron transport calculations was used in the activation calculations. The activation analysis was performed using the activation code DKR-PULSAR2.0. The code combined the neutron flux with the FENDL/A-2.0 data library to calculate the activity and decay heat as a function of time following shutdown. Calculated specific activities were used to calculate the waste disposal ratings (WDR) of the different

Table 11.6.1–1 Elemental Composition of the W-5Re Alloy

Nuclide	wt% or wppm
H	5 wppm
C	30 wppm
N	10 wppm
O	30 wppm
Na	10 wppm
Mg	5 wppm
Al	15 wppm
Si	20 wppm
P	50 wppm
S	5 wppm
K	10 wppm
Ca	10 wppm
Ti	10 wppm
Cr	10 wppm
Mn	5 wppm
Fe	30 wppm
Co	10 wppm
Ni	20 wppm
Cu	10 wppm
Zn	5 wppm
As	5 wppm
Zr	10 wppm
Nb	10 wppm
Mo	100 wppm
Ag	5 wppm
Cd	10 wppm
Ba	10 wppm
Ta	10 wppm
W	94.96%
Re	5 %
Pb	10 wppm

components at the end of their lifetime. Results of the decay heat analysis were used to calculate the temperature variation exhibited by the structure during a loss of coolant accident (LOCA).

11.6.2 activity and decay heat — Figures 11.6.2–1 and 11.6.2–2 show the specific activity and decay heat values induced in the different components as a function of time following shutdown, respectively. As shown in the two figures, the W-5Re alloy produces high level of radioactivity after shutdown. The first wall and blanket dominate the overall activity and decay heat induced in the structure. Table 11.6.2–1 shows a list of nuclides that dominate the induced radioactivity in the different components. As shown in the table, ^{181}W ($T_{1/2} = 121$ day), ^{185}W ($T_{1/2} = 75.1$ day), and ^{184}Re ($T_{1/2} = 38$ day) are the main contributors to the induced radioactivity during the first few weeks following shutdown. Neutron interactions and subsequent decays of both tungsten

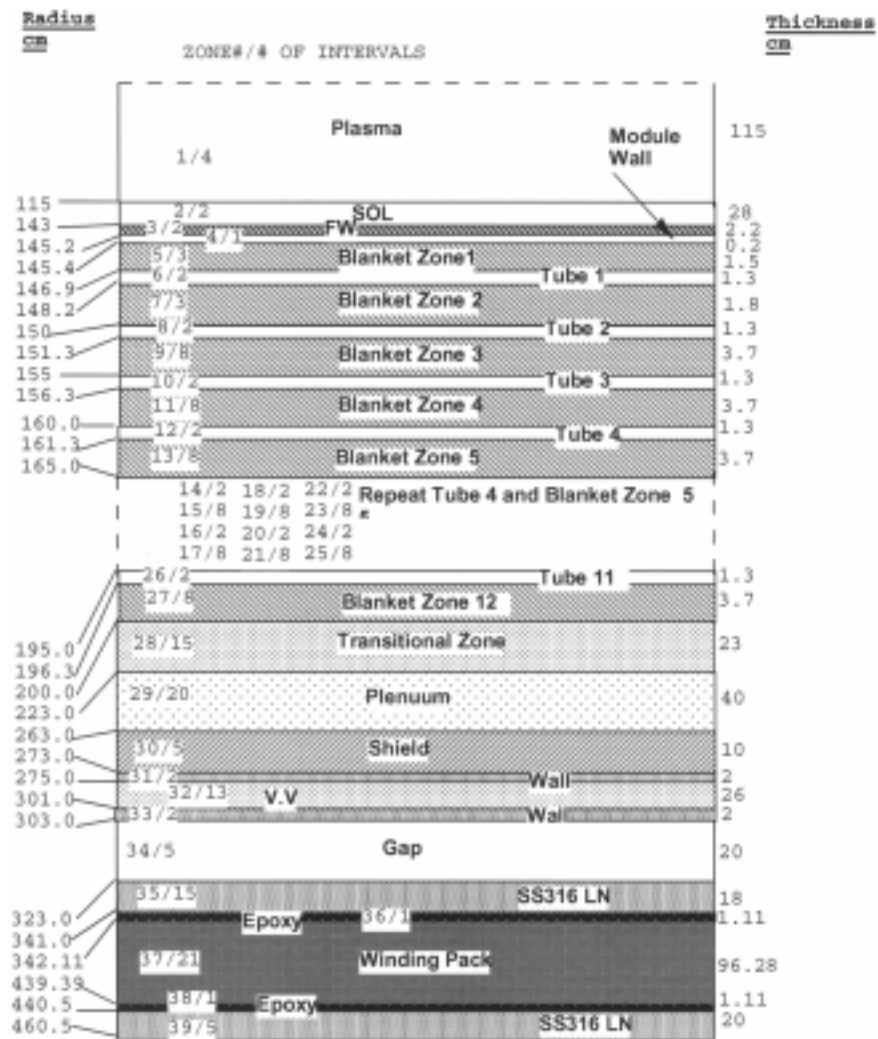


Fig. 11.6.2–1 Activity induced in the different components as a function of time following shutdown.

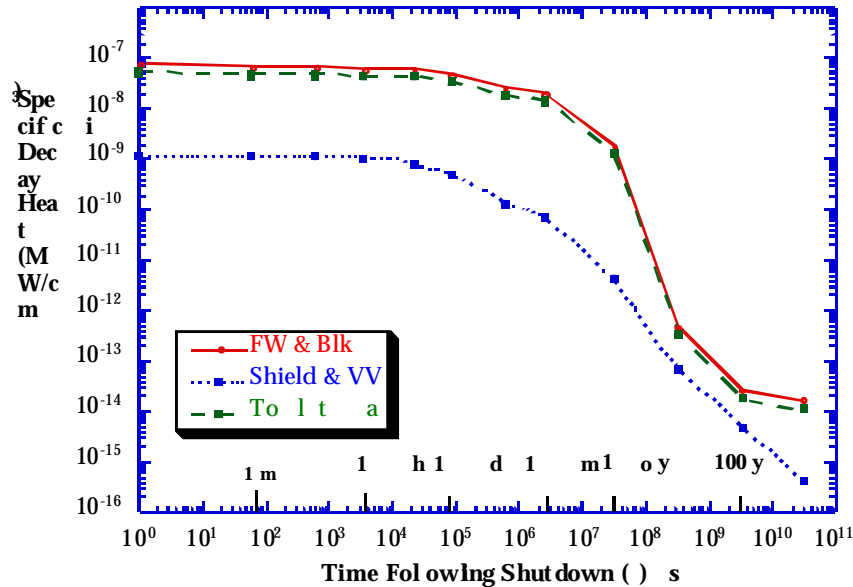


Fig. 11.6.2–2 Decay heat induced in the different components as a function of time following shutdown.

and rhenium produce these isotopes. The long-term radioactivity (between one and 10 yr) is generated by the ^{179}Ta ($T_{1/2} = 665$ day), ^{182}Ta ($T_{1/2} = 115$ day), and $^{186\text{m}}\text{Re}$ ($T_{1/2} = 2 \times 10^5$ yr) isotopes. Out of these three isotopes, $^{186\text{m}}\text{Re}$ is the most troublesome because it is considered as a major contributor to the WDR at the end of the plant lifetime. In addition, $^{186\text{m}}\text{Re}$ is also one of the main contributors to the off-site doses during an accident. Nuclides with much longer half-lives have no impact on the decay heat generated from the LOCA point of view. However, as shown in the next section, these nuclides dominate the WDR.

Table 11.6.2–1 List of Dominant Nuclides

	Activity	Decay Heat
Short term < 1 day	^{185}W , ^{181}W	^{184}Re , ^{185}W
Intermediate term < 1 month	^{181}W , ^{185}W	^{184}Re , ^{185}W
Long term > 1 yr	^{179}Ta , $^{186\text{m}}\text{Re}$	^{182}Ta , $^{186\text{m}}\text{Re}$

11.6.3 waste disposal ratings — The radioactive waste (radwaste) of the different components of the machine was evaluated according to both the NRC 10CFR61 [11.6.3–1] and Fetter waste disposal concentration limits [11.6.3–2]. The 10CFR61 regulations assume that the waste disposal site will be under administrative control for 100 yr. The dose at the site to an inadvertent intruder after the 100 yr is limited to less than 500 mrem/yr. The WDR is defined as the sum of the ratio of the concentration of a particular isotope to the maximum allowed concentration of that isotope and sum over all isotopes and for a particular class. If the calculated WDR (1 when Class A limits are used, the radwaste should qualify for Class A segregated waste. The major hazard of this class

of waste is to individuals who are responsible for handling it. Such waste is not considered to be a hazard following the loss of institutional control of the disposal site. Similar calculation can be done for Class C waste. The WDR is (1 when Class C limits are used; the waste is termed Class C intruder waste. It must be packaged and buried such that it will not pose a hazard to an inadvertent intruder after the 100 yr institutional period is over. Class C waste is assumed to be stable for 500 yr. Using Class C limits, a WDR > 1 implies that the radwaste does not qualify for shallow land burial.

Fetter developed a revision of the NRC’s intruder model to calculate waste disposal limits for a more complete coverage of long-lived radionuclides that are of interest for fusion researchers than the limited number of radionuclides that are covered in the current 10CFR61 regulations. Fetter’s model included more accurate transfer coefficients and dose conversion factors. However, while the NRC model limits the whole body dose to 500 mrem or the dose to any single organ (one of seven body organs) to 1.5 rem, Fetter limits are based on the maximum dose to the whole body only.

Specific activities calculated by the DKR-PULSAR2.0 code were used to calculate the WDR. The WDR for the Fetter and 10CFR61 limits are shown in Tables 11.6.3–1 and 11.6.3–2, respectively. Results in the tables are given for compacted wastes. Compacted waste corresponds to crushing the solid waste before disposal (to eliminate voids in the structure) and thus disallowing artificial dilution of activity. The Class C WDR was calculated after a 1-yr cooling period. The dominant nuclides are given between brackets.

Table 11.6.3–1 Class C Waste Disposal Ratings Using Fetter Limits

Zone	FPY	WDR	Dominant Nuclides
FW	5	43.1	^{186m} Re, ^{108m} AG, ⁹⁴ Nb
Module wall	5	39.7	^{186m} Re, ^{108m} Ag, ⁹⁴ Nb
Blanket	5	11.9	⁹⁴ Nb, ^{108m} AG, ^{186m} Re
Transitional zone	5	1.54	⁹⁴ Nb, ^{108m} Ag
Plenum	5	0.224	⁹⁴ Nb
Shield	30	0.228	⁹⁴ Nb
W	30	9.15x10 ⁻²	^{192m} Ir, ⁹⁴ Nb

As shown in Table 11.6.3–1, according to Fetter limits, the first wall, module wall, blanket, and transitional zone would not qualify for disposal for Class C waste. As a matter of fact the W-5Re alloy produce such a high activity that the first wall would have a WDR which is an order of magnitude higher than the Class C WDR limits. The higher WDR is due to the contribution from ^{186m}Re, ^{108m}AG, and ⁹⁴Nb isotopes. Only ^{186m}Re is a product of nuclear interactions with base elements in the W-5Re alloy. The other isotopes ^{108m}AG(T_{1/2} = 130 yr), and ⁹⁴Nb(T_{1/2} = 20,000 yr) are produced by nuclear interactions with the niobium and silver impurities present in the W-5Re alloy used in the analysis. Finally, as sown in Table 11.6.3–2, according to

the 10CFR61 limits, the first wall, module wall, blanket, and transitional zone also would not qualify for disposal as Class C waste. In this case, the waste disposal ratings of all components are dominated by contribution from the ⁹⁴Nb isotope.

Table 11.6.3–2 Class C Waste Disposal Ratings Using 10CFR61 Limits

Zone	FPY	WDR	Dominant Nuclides
FW	5	6.34	⁹⁴ Nb
Module wall	5	6.2	⁹⁴ Nb
Blanket	5	3.22	⁹⁴ Nb
Transitional zone	5	1.01	⁹⁴ Nb
Plenum	5	0.188	⁹⁴ Nb
Shield	30	0.2	⁹⁴ Nb
W	30	2.07x10 ⁻²	⁹⁴ Nb

11.7 Power Conversion System

The major incentive for employing high-temperature refractory alloy first wall and blanket with helium cooling in this design is to enable direct coupling with a close-cycle gas turbine (Brayton Cycle) for high efficiency power conversion. In this argument, the high-pressure helium coolant is used directly as the working fluid for the PCS. This has the advantage of eliminating an intermediate high-temperature He/He HX which would be a significant technical challenge. On the other hand, the potential for tritium contamination in the PCS must be addressed and appropriate design measures must be taken to prevent further spread of contamination and to facilitate maintenance of PCS components.

Because thermal efficiency is a high-leverage parameter with respect to COE in any power conversion device, the system configuration and process parameters were aggressively selected to maximize gross electric output. Figure 11.7–1 shows the process flow arrangement of this power conversion system.

Hot helium from the first wall and blanket is expanded over the turbine with a ~2-to-1 pressure ratio (Pr). The Pr is an independent variable and can be selected to optimize efficiency or to accommodate special temperature conditions as described below. The turbine uses cast nickel alloy blades with internal helium cooling similar to common gas-fired gas turbines which operate above 1250°C. However, inlet structure will also require insulation/cooling depending on the physical layout. An adiabatic efficiency of 93% is achievable with ~10 blading stages.

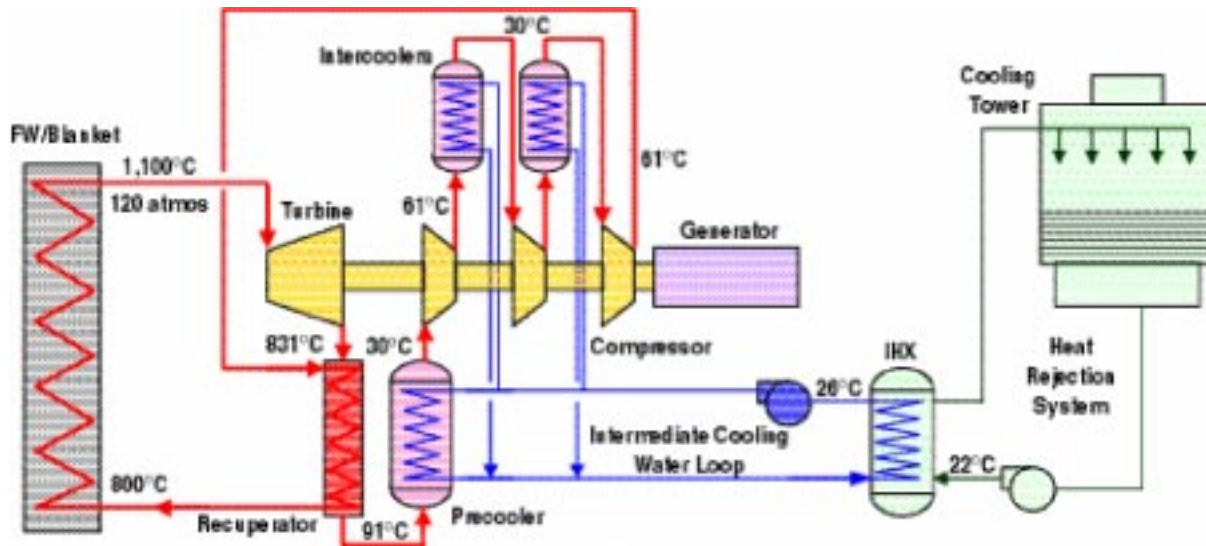


Fig. 11.7-1 Power conversion system process arrangement.

Helium from the turbine exhaust flows through the recuperator, which recovers the heat energy, which is no longer suitable for economic conversion to work but can be transferred to the high-pressure side of the cycle. The recuperator is a plate fin HX with specially developed surface enhancement for high effectiveness. Recuperator effectiveness is one of the most sensitive parameters in overall PCS performance. Large, high-alloy, recuperators with 95% effectiveness are state of the art and a few smaller recuperators with 96% effectiveness have been built. For this study, 96% effectiveness was assumed.

From the recuperator, the helium flows through the precooler to the series of compressor/intercooler segments. The precooler is tube/shell HX with surface-enhanced, water-filled tubes. The compressor is located on the same shaft as the turbine in counter-thrust arrangement. The compressor is divided into three sections to allow for two stages of intercooling. Each compressor section has ~7 blading stages giving a net adiabatic efficiency of 88%. The intercoolers are water-cooled HXs similar in design to the precooler. The purpose of the precooler and intercoolers is to reduce the helium volumetric flow to the compressors in order to reduce the parasitic compressive work. The helium from the compressor is routed back through the recuperator (cold-side) and then to the first wall and blanket inlet.

Additional features of the PCS include a synchronous 20 kV generator on the same shaft as the turbo-compressor. The generator can be submerged in helium so that the entire PCS can be hermetically sealed to prevent leakage of helium and any tritium contamination. Tritium release is also prevented by an intermediate water-cooling loop between the precooler/intercoolers and the heat rejection system (cooling tower).

Selection of the main PCS process parameters has been done in concert with the selection of the first wall and blanket materials and design features. The principal interface variables are the first wall and blanket outlet/inlet temperatures. First wall and blanket materials have been selected to give the highest possible outlet temperature which, in turn, maximizes PCS efficiency. The inlet temperature is determined as a balance between required first wall and blanket flow rates and PCS

efficiency. Helium pressure has a secondary effect on PCS efficiency and is selected mainly from the standpoint of first wall and blanket flow and pressure drop considerations.

Figure 11.7–2 shows the effect of variation of first wall and blanket outlet temperature and pressure on PCS performance for the selection system configuration. The curves shows sharp increases in gross efficiency with temperature but are relatively flat with respect to pressure. The curves are based on optimum inlet temperatures. Figure 11.7–3 shows the effect of first wall and blanket inlet temperature variation on PCS performance for the selected outlet temperature of 1100°C. The effect of increasing the inlet temperature from an optimum value of 700° to 800°C is roughly a one-point efficiency loss.

No work has been done on the system physical arrangement or location. However, the physical arrangement is somewhat flexible such that the physical arrangement of the heat source can be designed relatively independently of the PCS. Based on reasonable extrapolations from the current state of the art for large turbine machine design, the maximum output of a single unit is about 400 MWe. Thus, five PCS units will be required.

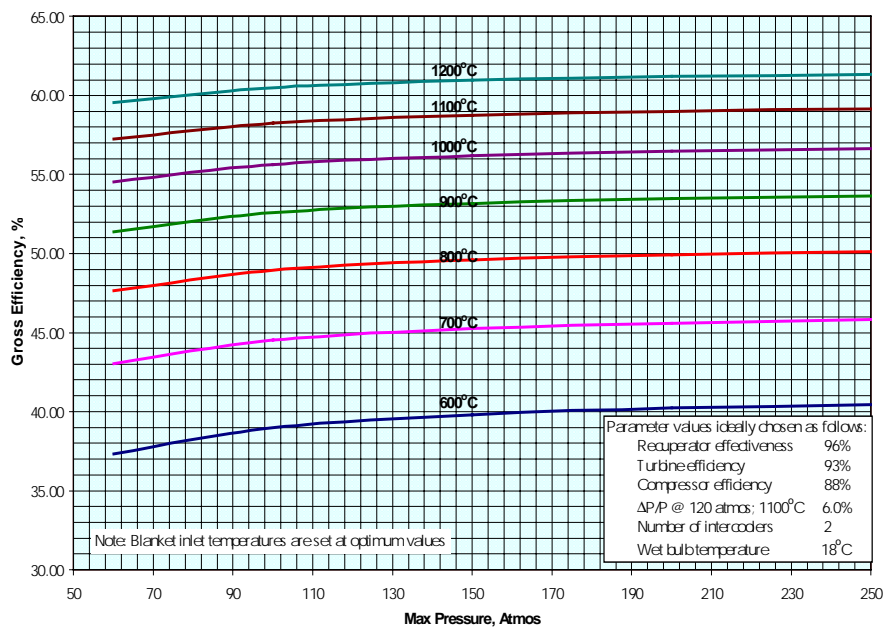


Fig. 11.7–2 Effect of first wall and blanket outlet temperature.

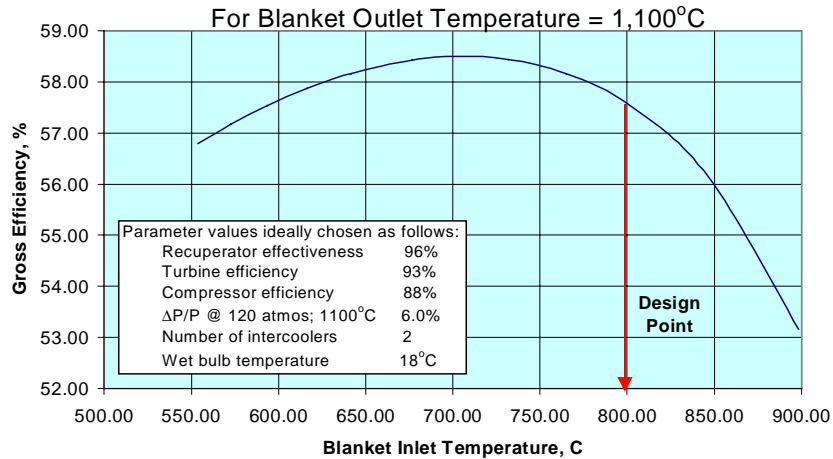


Fig. 11.7–3 Effect of first wall and blanket inlet temperature on PCS gross efficiency.

Figure 11.7–3 shows the effect of first wall and blanket inlet temperature variation on PCS performance for the selected outlet temperature of 1100°C. Based on this, the selected gross efficiency for the preliminary design is 57.5%.

11.8 Tritium Migration and Control

Tritium produced in the lithium has to be recovered with an acceptable tritium inventory. The design goal of the tritium recovery system for lithium is usually to limit the tritium concentration to about 1 appm. This goal is to limit the total tritium inventory in the lithium to less than 200 g. The 200 g tritium inventory in one processing system is the approximate safety limit set for the ITER.

Many processes have been proposed to recover tritium from lithium. A recent proposal is to recover tritium by a cold trap process. [11.8–1]. The cold trap process was demonstrated to recover tritium from lithium to the saturation concentration [11.8–2]. However, the saturation tritium concentration at 200°C is about 250 appm, and this far exceeds the design goal of 1 appm. The new proposal is to add protium to the lithium. By maintaining the total hydrogen concentration at the saturation limit of 250 appm, the tritium concentration can be below 1 appm. The design of the process and the cost associated with the separation of T from H was calculated by ITER and was judged to be acceptable.

The proposed lithium flow rate for the tritium recovery is 20 Kg/s. This is a very small flow rate and has to be distributed uniformly over all the blanket modules. The mechanical design of lithium flow control from all regimes within the blanket will be a challenge. If the lithium flow rate is nonuniform, the total tritium inventory will increase due to the locally high concentration of the tritium. Therefore, it can be expected that the tritium inventory will be higher than the design value due to his local “hot spot” effect. The total first wall and blanket tritium inventory will have to be assessed in more detail.

Tritium will permeate to the He coolant both by pressure driven from the lithium and by plasma-driven permeation across the first wall. The best estimate is that the plasma-driven effect

will dominate the tritium permeation. The permeation rate is estimated to be 10 g per full power day. Therefore, a tritium clean up system will be required. To recover tritium from the helium gas to a very low concentration is difficult. If a steam generator is used for power conversion, a tritium partial pressure at the up stream of the steam generator has to be less than 10^{-7} Pa to limit tritium permeation to the steam side to less than 10 Ci/d [11.8–3]. Therefore, the tritium concentration in the He has to be 10^{-5} appb. Therefore, the tritium permeation to the steam side can be a major design issue if a steam power cycle is used.

For this design, there is no high temperature HX located at the outside. The only high temperature, large HX is the recuperator, which is from primary helium to the primary helium, as shown on Fig. 11.7–1. The only external HX is the one to heat sink, which is at a low temperature, and has much smaller heat transfer surface area. Therefore, the allowable tritium concentration in the helium can be much higher than the PCS design that uses a steam generator. Higher tritium concentration in the helium stream will ease the tritium clean up requirement of the helium coolant.

Recent experimental results from TSTA [11.8–4] show that a permeation window can be used for tritium clean up from gas. This process is capable of removing tritium from gas to a pressure of about 1 Pa. Since permeation is not a critical issue for this first wall and blanket design, 1 Pa tritium partial pressure would be acceptable. The effect of this tritium partial pressure to the operation of the pumps and valves will have to be assessed.

Another alternative for removing tritium from He is by using liquid nitrogen-cooled molecular sieve beds. This process has been demonstrated to be effective for this purpose at practical scale at TSTA. The results showed that hydrogen isotopes could be removed so that there was none detectable at the bed outlet using gas chromatography. This detection limit is about 1 ppm.

11.9 Safety

The use of tungsten as the structural material in this first wall and blanket concept poses some safety challenges. Tungsten is a radiologically hazardous material with high decay heat as shown in Section 11.6.3, so we must ensure that the design is such that long-term accident temperatures are low enough that unacceptably large amounts of tungsten are not mobilized during an accident.

Because this design is in a preliminary stage, the purpose of this safety evaluation was to look for “show-stoppers,” situations where it is doubtful that safety requirements can be met. Chapter 4 (Evaluation Criteria) gives general safety guidelines; and although these are not hard limits, they provide guidance for designs in early stages.

11.9.1 loss of coolant accident (LOCA) calculations — A series of LOCA calculations were done to estimate long-term temperatures and provide guidance to designers to help them make the design better from a safety point of view (*e.g.*, provide good heat transfer paths that will limit long-term LOCA temperatures). The radial build used in the decay heat calculations and subsequent LOCA calculations is shown in Fig. 11.5.2–1. Figure 11.9.1–1 shows the decay heat

assuming an all tungsten structural, and compares it with a material such as vanadium which has a lower decay heat by a factor often.

Calculations using the CHEMCON code [11.9.1–1] showed that a LOCA, with no safety-grade cooling systems (therefore no active cooling), resulted in temperatures in excess of 900°C during the entire accident (see Fig. 11.9.1–2). As indicated in Chapter 4 (Evaluation Criteria), a general guideline is that long-term temperatures should be below 800°C to minimize the contribution to the activation product source term from oxidation-driven mobilization. Figure 11.9.1–3 shows the first wall temperatures assuming an all-vanadium structure. Although overall temperature is lower, temperatures as a function of time are in excess of 900°C during the entire accident. The initial temperature spike is due to the disruption at the beginning of the accident.

These calculations indicate that a safety-grade cooling system may be needed to ensure that accident temperatures are low enough to satisfy safety requirements. Safety grade systems are assumed to operate under accident conditions. Two options were considered: the VV cooling system and the tritium extraction system (with a flow rate of 20 kg/s). Figure 11.9.1–4 shows the first wall temperatures for these scenarios. The tritium extraction system is the more efficient method for heat removal, it removes the heat closer to the source and does not rely on radiative heat transfer across the gap between the plenum and VV. With the tritium extraction system operating, long-term accident temperatures remain below 800°C.

The tritium extraction system may result in a higher tritium concentration than is provided by this scenario to extract the tritium efficiently. It may be necessary to segment the coolant in the blanket region radially, and use most of the 20 kg/s flow rate for the lithium in the front of the blanket (where the tritium concentration is highest). Because the decay heat is also higher in the front part of the blanket, this should adequately remove the decay heat, but further calculations and modeling will be necessary to confirm this design approach.

The next step in this type of analysis is to calculate the amount of tungsten mobilized during a postulated accident and the corresponding off-site dose. This gives an indication of the confinement necessary to ensure that safety doses limits can be met. These calculations will be documented in the next report.

11.9.1.1 other safety issues and reliability issues — Because liquid lithium is present in this design to provide tritium breeding, the design suggestions outlined in Chapter 4 should be followed. As more design detail becomes available, further safety analyses will be done to ensure that safety requirements are met. Similarly, a reliability assessment cannot be done until more design detail is available; however, general information on reliability issues can be found in Chapter 4.

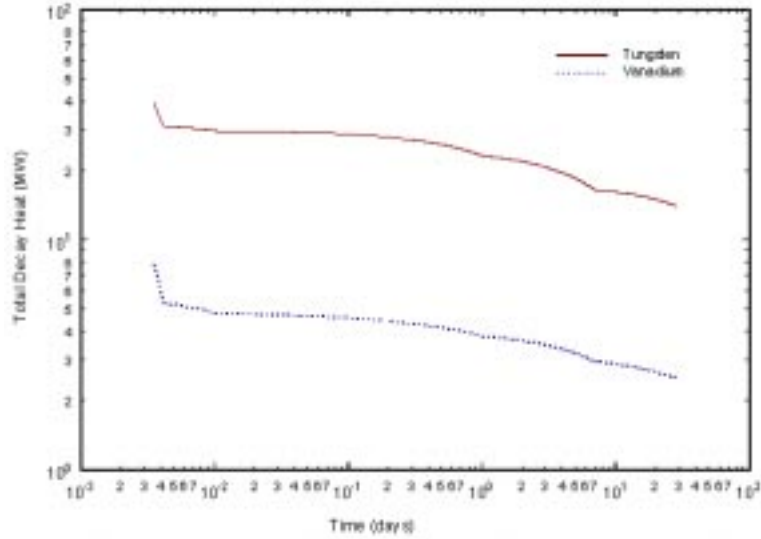


Fig. 11.9.1-1 Decay heat values in the outer radial build were normalized to approximate V structural material in place of W and provide a lower bound for decay heat values

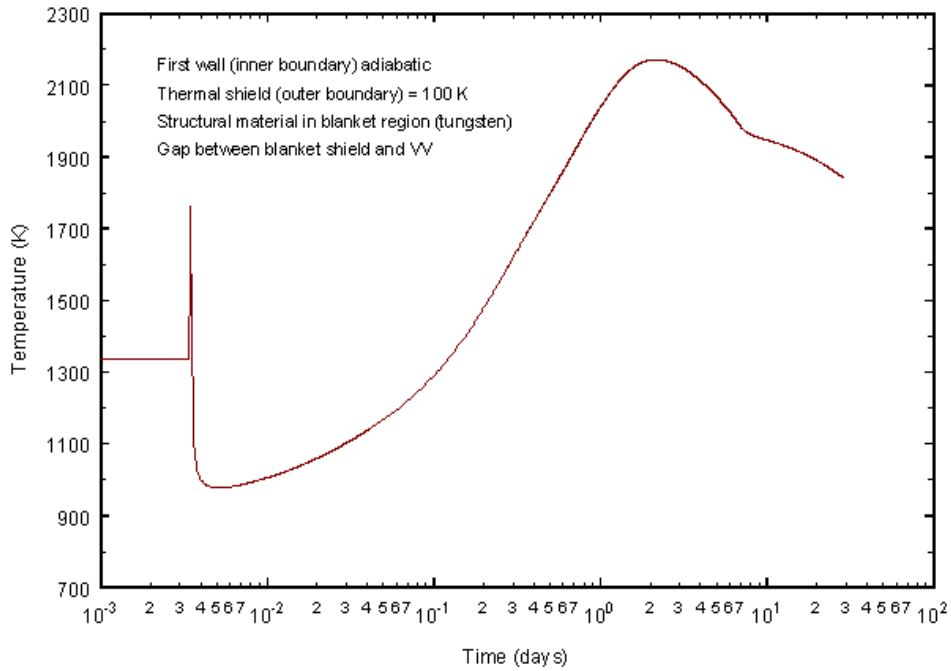


Fig. 11.9.1-2 First wall temperature assuming no active cooling during LOCA, all tungsten structure.

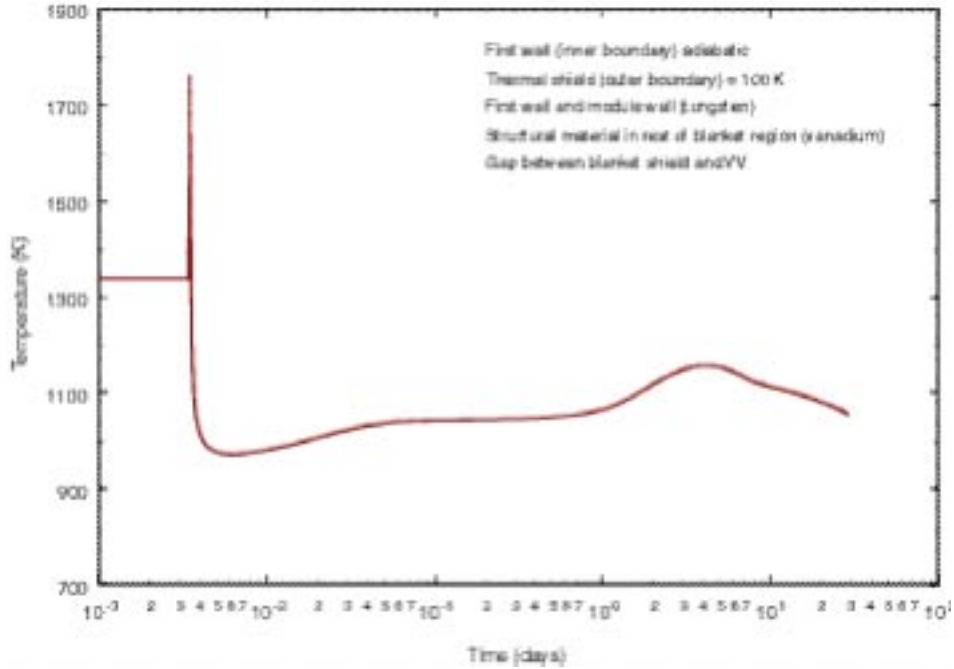


Fig. 11.9.1–3 First wall temperature assuming no active cooling during LOCA, all vanadium structure.

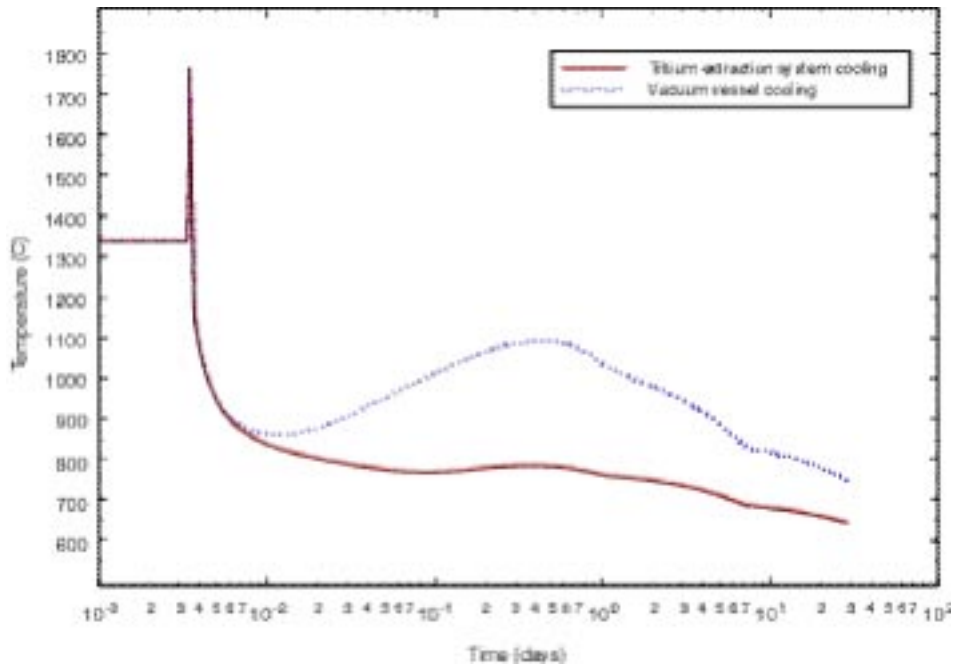


Fig. 11.9.1–4 First wall temperature for two scenarios: VV cooling operates during LOCA, and tritium extraction system operates during LOCA.

11.10 system design — Based on the W-alloy first wall and blanket design, we assessed the tokamak technical and economic performance of a superconducting tokamak reactor. A fusion

reactor system code developed by General Atomics was then used to project the COE [11.10–1]. This system code uses ARIES–RS [11.3.1.1–1] and ARIES–ST [11.10–2] as reference design points, and the performance of superconducting and normal conducting coil tokamak reactors can be projected for difference aspect ratio, power output and neutron wall loading. Based on the results from plasma equilibrium calculations, the key physics design parameters of β_N , β_p , β_t , and κ were calculated for A = 4 design. For protection from radiation damage, the selected inboard standoff distance is 1.3 m. Similar to the ARIES–RS design, a central column current density of 31 MA/m² was used. It is observed that the fusion power core component life will be a function of maximum Γ_n , and frequent change out will have a negative impact on reactor availability. To account for this effect a simplified availability model is included. This model is based on the following assumptions: the material fluence limit of 15 MW.a/m², a reactor life of 30 yr, a FW/blanket change out time of three months, the other necessary total down time of 72 months, and that we can achieve an availability of 75% when the maximum Γ_n is at 4 MW/m². The variation of availability as a function of maximum neutron wall loading (Γ_{n-max}) can then be represented by

$$\text{Availability} = 288/(360+6*\Gamma_{n-max}) \quad .$$

Where Γ_{n-max} is the maximum neutron wall loading and the fusion power core components lifetime is assumed to be 15 MW.a/m².

Since at this time we are not able to project the acceptable power output of fusion reactor that the utility in the future will be interested in, we took advantage of the economy of scale and designed our reference power output at 2 GWe. This is not unreasonable since the fission reactors have been increasing the power output from a few hundred MWe to >1400 MWe already.

Based on the projected gross thermal efficiency of 57.5%, in order to limit the power output to no higher than 2 GWe, the maximum neutron wall loading only needs to be operated at 7.49 MW/m², with a corresponding maximum first wall heat flux of 2.16 MW/m². The physics and costing results are given in Table 11.10–1. In summary, at the thermal efficiency of 57.5%, a superconducting reactor with an aspect ratio of 4 and an output power of 2 GWe is projected to have a total COE of 54.6 mill/kWh, including replacement of fusion power core components of a 30-yr life fusion reactor. It should be noted that the cost of W-alloy components is highly uncertain. The assumption made was that as a 10th of a kind reactor, the first wall and blanket would be similar to the cost of the V-alloy first wall and blanket components of the ARIES–RS reactor design [11.3.1.1–1].

**Table 11.10–1 Design Parameters of a
2 GWe A=4 Superconducting Coil Tokamak Reactor Designs
(Kr is Used for Enhanced Radiation)**

Net electrical power, MWe	2005
Plasma aspect ratio, A	4
Plasma vertical elongation	1.769
Minor plasma radius, a, (m)	1.442
Major toroidal radius, R ₀ , (m)	5.767
Plasma volume, (m ³)	393.7
First-wall surface area, (m ²)	483.4
<i>Number of FW/Blanket sector</i>	<i>16</i>
<i>Number of modules per sector</i>	<i>3</i>
Midplane outboard module width, (m)	0.941
Module height, (m)	6.1
<i>Blanket energy multiplication</i>	<i>1.18</i>
Average neutron wall loading, MW/m ²	5.35
Average first wall surface heat flux, MW/m ²	1.55
Peaking factor	1.4
Kr fraction of electron density	0.0009
Divertor: (double null)	
Strike point foot print width, (m)	0.1
Divertor plate to B-field incline angle, °	20
Divertor heat flux, MW/m ²	2.11
Blanket thickness, m	1.2
W-density, kg/m ³	19300
W-alloy unit cost, \$/kg	100
<i>FW/blanket cost, \$M</i>	<i>116</i>
Fast wave current drive power, MW	85.3
TF coil current density, MA/m ²	31
Bt, T	9.61
Fusion power, (MW)	3372
Thermal power, MWth	3975
CCGT Thermal η _{th} , %	57.5
Availability @ 4 MW/m ² =75%	71.1%
Turbine system cost, \$M	381
Total COE, (mill/kWh) ^(a)	54.6

^(a)Total COE includes the cost of first wall and blanket replacement for a 30 yr life fusion power plant.

11.11 Key Issues and R&D

We have completed the preliminary evaluation of a helium-cooled refractory alloy first wall and blanket design. Many development issues are identified in different areas. The following is a preliminary list of key issues, grouped by areas that will have to be addressed in order to make it to become a viable design.

- Materials:
 - Irradiated and engineering design material properties of W-alloy
 - Design criteria for W-alloy
 - Fabrication of W-alloy components
 - Minimum cost of W-alloy components including material and fabrication
 - Compatibility between helium impurities and W-alloy
- Design:
 - External coolant piping routing
 - Structure support to handle thermal expansion
 - High temperature piping
 - Develop robust high performance fusion power core W-alloy components
- Thermalhydraulics:
 - Helium flow control, distribution and stability
 - First wall and blanket temperature management and startup
- Nuclear analysis:
 - 3-D assessment
- Safety:
 - Removal of afterheat during LOCA and LOFA
- Plasma and surface interaction:
 - W-surface compatibility with high performance plasma
- Tritium:
 - Extraction, inventory and PCS contamination

In addition, the availability of fusion power core components will have to be demonstrated.

11.12 Conclusions

We completed the preliminary design of a high performance He-cooled W-5Re alloy first wall and blanket design. A separate first wall, pool lithium configuration was selected. Due to the lack of irradiated data, conservative assumptions on selecting the W-alloy properties were used. Compatibility of W-alloy and oxygen impurities in the helium was assessed. Commercial solid gettering modules can be used to maintain the impurity level to <1 appm. Potentially, based on the results of selected analyses on key structural loading locations, the outboard first wall and blanket design could meet the material temperature and structural design limits provided that the peak structural loading from disruption could be mitigated. Based on the outboard blanket

configuration, the 1-D cylindrical model tritium breeder ratio of 1.43 can be reached with a Li-6 enrichment of 35%. But the presence of induced radioactivity will not allow the W-5Re alloy components to meet the criteria of low-level waste mainly due to the presence of alloying element Re and impurities. W-alloy will generate a high level of afterheat, with the tritium extraction system operating, long-term accident temperatures could be designed to remain below 800°C. Cold trap process with the addition of protium to the lithium could be used for tritium extraction. At the CCGT gross thermal efficiency of 57.5%, a superconducting reactor with an aspect ratio of 4 and an output power of 2 GWe is projected to have a COE of 54.6 mill/kWh. This is based on the assumption that the W-alloy components will have total cost similar to the V-alloy components of the ARIES-RS design. Critical issues were identified and we plan to continue the evaluation on some of the critical issues during the next phase of the APEX design study.

11.13 Information Required for Scientific Evaluation

The minimum information required for each concept to facilitate performing the scientific evaluation has been identified. Although no detailed analysis is expected in the early stage of the concept development, the design parameters required are essential for the evaluation process and could be based on preliminary scoping analysis. The required information is listed below.

- Sketches of the geometry of the in-vessel components
- Figures 11.3.2–5
- Outline of outboard First wall and blanket/shield radial build including approximate dimensions
- Figures 11.3.2–5 and 11.3.2–6
- Candidate materials for PFC, structure, breeder, and coolant
- Structural material: W-5Re alloy
- Breeder: Liquid lithium
- Coolant: Helium at 12 MPa
- Estimated values of the following parameters, based on a peak neutron wall loading of 10 MW/m², a peak surface heat flux of 2 MW/m², and a peaking factor of 1.4 for both:
 - At 2 GWe power output, and thermal efficiency of 57.5%, the peak neutron wall loading is 7.49 MW/m², peak surface heat flux of 2.16 MW/m². If the reactor is designed to 10 MW/m², the reactor power would be >> 2 GWe. The corresponding COE would be reduced, but the power output could be too large.
- Coolant parameters (temperature, pressure) at inlet/outlet of: 800°C/1100°C.
- Plasma facing surface (liquid FW) NA

- FW cooling channel (solid FW) 1074°C/1240°C.
- Breeding zone- 1152°C/1229°C
- Maximum/minimum temperatures of
- Breeder material 1152°C/1245°C
- Structural material 1028°C/1202°C
- Maximum primary and total (primary+secondary) stress in the structural material
- 95 MPa
- Tritium breeding ratio
- (Overall TBR estimated from local 1-D major axis calculations with heterogeneity, volume fractions represented by the outboard first wall and blanket)
- ~1.43 when Li-6 enrichment is ~35%.
- Maximum power density in structure, breeder and coolant material
- W-alloy-69.2 W/cc
- Lithium breeder –30 W/cc
- Energy multiplication in in-vessel components
- 1.18
- Maximum structure damage
- He, Fig. 11.5.5.1–3, H, Fig. 11.5.5.1–5, dpa, 56.3 @ 10 MWa/m²
- Structure activity, decay heat, and radwaste classification
- Specific activity, Fig. 11.6.2–2, decay heat, Fig. 11.6.3
- Fetter limits WDR for Class C >1:FW, module wall, blanket, transition zone
- Class C < 1: Plenum, shield, VV
- For a typical unit size module, which could be one of the following elements:
- (Include the sketch of coolant routing)
- A chunk with a first surface of 1m²

- Fig. 11.3.2–5
- A cut out of a blanket segment with a poloidal height of 1m
- Fig. 11.3.2–5
- A sector cut of a segment with full height and a toroidal width of 1m
- NA
- A complete outboard segment
- NA
- A full sector
- Fig. 3.1
- Estimates for the following parameters have to be provided, assuming the heat loads given under D):
 - a. total surface heat load
744.6 MW
 - b. total heat load (surface heat load + volumetric heat generation)
3975 MW
 - c. coolant mass flow rate (either total or for the different zones, depending on the concept)
2552 kg/s
 - d. coolant velocities in first wall and breeding zone
First wall: 57 to 65 m/s, breeder: 68 to 81 m/s
 - e. coolant inlet and outlet manifold sizes
Per vertical module:
Outboard, 48 modules: diam.-in-19 cm, diam.-out-22 cm.
Inboard, 32 modules: diam.-in-18 cm, diam.-out-21 cm
 - f. coolant inlet and outlet piping location and sizes

TBD depends on the division of piping. Inlets and outlets are located at the top of the modules.

- g. coolant pumping power

324 MW

- h. a brief indication of structural support needed

Each module is support on the VV with gradual and flexible supports to accommodate thermal expansion.

- i. identification of external primary or secondary coolant pumping system

CCGT also acts as the helium circulator.

References

- [11.3.1.1–1] M.S. Tillack, Special Issue, *Fusion Engineering and Design* **38**, 1–218 (1997).
- [11.3.2–1] “Blanket Comparison and Selection Study,” Argonne National Laboratory Report ANL/FPP-83-1 (1983).
- [11.3.2–2] C.P.C. Wong, *et al.*, “A Robust Helium-Cooled Shield/Blanket Design for ITER,” 15th IEEE/NPSS Symp. on Fusion Engineering, October 11–15, 1993, Hyannis, Massachusetts, Vol. 1, p. 13 (Institute of Electrical and Electronics Engineers, Inc., Piscataway, New Jersey, 1994).
- [11.4–1] M.S. Tillack *et al.*, “Helium-Cooled Divertor for ITER: A Study of Cooling Options, Requirements and Limits,” ITER Report published by UCLA Report No. UCLA-FNT-67 UCLA-ENG-93-22 (1993).
- [11.4–2] F. Najmabadi *et al.*, “The ARIES-I Tokamak Reactor Study, Final Report,” University of California, Los Angeles, Report UCLA-PPG-1323 (1991).
- [11.4.3–1] M.T. North and J.H. Rosenfeld, “Test Results from a Helium Gas-cooled Porous Metal Heat Exchanger,” Khonsary, ed., *High Heat Flux Engineering III*, Vol. 2855 (1996) ISBN 0-8194-2243-6.
- [11.4.3–2] D.L. Youchison and J. M. McDonald, “Thermal Performance and Flow Instabilities in a Multi-channel, Helium-cooled, Porous Metal Divertor Module,” to be published in *Proc. Int. Symp. on Fusion Technology*, September 19–24, 1999, Rome, Italy.
- [11.4.3–3] D.L. Youchison, M. G. Izenon, C. B. Baxi, J. H. Rosenfeld, “High Heat Flux Testing of Helium-Cooled Heat Exchangers for Fusion Applications,” *Fusion Technology* **29**, 559 (1996).
- [11.4.3.1–1] H. Kurishita *et al.*, “Effect of Neutron-Irradiation on Low Temperature Toughness of TiC-Dispersed Molybdenum Alloys,” *J. Nucl. Mater.* **239**, 253 (1996).
- [11.4.3.1–2] H. Kurishita *et al.*, “Development of Mo Alloys with Improved Resistance of Embrittlement by Recrystallization and Irradiation Molybdenum Alloys,” *J. Nucl. Mater.* **237**, 557 (1996).
- [11.4.3.1–3] K. Tokunaga *et al.*, “High Heat Load Properties of TiC-dispersed Mo Alloys,” *J. Nucl. Mater.* **241**, 1197 (1997).
- [11.4.3.2–1] J. Sherman, R.H. Tuffias and R.B. Kaplan, “Refractory Ceramic Foams: A Novel, New high Temperature Structure,” *Ceramic Bulletin* **70**, 1025 (1991).
- [11.4.4–1] C. Baxi and C. Wong, “Review of Helium Cooling for Fusion Reactor Applications,” to be published in *Proc. Int. Symp. on Fusion Technology*, September 19–24, 1999, Rome, Italy.

- [11.6.3–1] Nuclear Regulatory Commission, 10CFR part 61, “Licensing Requirements for Land Disposal of Radioactive Waste,” Federal Register FR 47, 57446 (1982).
- [11.6.3–2] S. Fetter, E. Cheng and F. Mann, “Long Term Radioactive Waste from Fusion Reactors,” Fusion Engineering and Design **13**, 239 (1990).
- [11.8–1] D.K. Sze, R.F. Mattas, J. Anderson, R. Haange, H. Yoshida, and O. Kveton, “Tritium Recovery Based on Cold Trap,” Proc. 3rd Int. Symp. on Fusion Nuclear Technology, June 1994, Los Angeles, California.
- [11.8–2] E. Veleckis and V.A. Maroni, “Thermodynamic Properties of Solutions in Hydrogen Isotopes in Metals and Alloys of Interest to Fusion Reactor Technology,” Proc. Int. Conf. on Radiation Effects and Tritium Technology for Fusion Reactors, October 1975, Gatlingburg, Tennessee.
- [11.8–3] D.L. Smith *et al.*, “Blanket Comparison and Selection Study – Final Report,” Argonne National Laboratory Report ANL/FPP-84-1 (1984).
- [11.8–4] S. Willms, Los Alamos National Laboratory, private communication.
- [11.9.1–1] M.J. Gaeta and B.J. Merrill, “CHEMCON User’s Manual Version 3.1,” INEL-95/0147 (1995).
- [11.10–1] C.P.C. Wong, R.D. Stambaugh, “Tokamak Reactor Designs as a Function of Aspect Ratio,” to be published in Proc. Int. Symp. on Fusion Technology, September 19–24, 1999, Rome, Italy.
- [11.10–2] R. L. Miller “Design Point Determination for the Commercial Spherical Tokamak, ARIES-ST,” Proc. 17th IEEE/NPS Symp. on Fusion Engineering, October 6–11, 1997, San Diego, California, Vol. 2, p. 1031 (Institute of Electrical and Electronics Engineers, Inc., Piscataway, New Jersey, 1998).